Title
Automation in Dental and Eye Surgery

Author
Wang, Haoran

Publication Date
2022

Peer reviewed|Thesis/dissertation

UNIVERSITY OF CALIFORNIA

Los Angeles

Automation in Dental and Eye Surgery

A dissertation submitted in partial satisfaction

of the requirements for the degree

Doctor of Philosophy in Mechanical Engineering

by

Haoran Wang

2022

ABSTRACT OF THE DISSERTATION

Automation in Dental and Eye Surgery

by

Haoran Wang

Doctor of Philosophy in Mechanical Engineering

University of California, Los Angeles, 2022

Professor Jacob Rosen, Chair

The advancing frontier of modern robotics has enabled the automation of dental implant surgery, which also invokes the problem of physical Human-Robot Interaction (pHRI) in the clinical environment. In this dissertation, the concern for pHRI is integrated into the design of a robot implant surgery system including identification of patient status, AI decisions upon patient status, and real-time control to execute decisions. The behavior of human surgeon and patient is investigated and a system structure that reacts to potential motion of the patient during the surgical tasks is proposed. The effectiveness of patient status identification and AI decision is verified via simulation and the control algorithm is simulated and tested with Denso VM industrial arm, ATI force sensor, Nobel Biocare OsseoSet drilling unit, Denso b-CAP and Microsoft Visual Studio C++ programming environment. A total of 9 sets of simulations and experiments are designed covering the 3 tracking

states plus 6 cases of switching among the 3 states. A prototype system is then built with control testing setup with an Microscribe MX digitizer and its behavior examined.

Robotic technology can take advantage of high precision and repeatability in boosting the quality of tooth preparation, but is facing problems in generating the trajectory with irregular shape of tooth under constraints of clinical considerations as well. The design of the trajectory must conserve as much original contour as possible while creating sufficient large margin for an effective and lasting crown. In the meanwhile, the high precision requirement of the robot arm prefers a small motion range while the limited oral space demands the tool to avoid collision with soft issues and adjacent tooth. In this dissertation, a full coverage tooth preparation trajectory is generated in axial reduction and occlusal reduction. The axial reduction trajectory conserves the original contour, creates a taper angle of 1.4^{o} and minimizes the robot motion range in the oral space. Two solutions are proposed for occlusal reduction. A V-shape cut prepares the tooth by following the principal direction to conserve the basic contour, and a topographic cut targets a maximum conservation of the original occlusal surface. The trajectories are tested by cutting a 3D printed model by air turbine driven handpiece, held by a Meca 500 robot. The test results verify that the trajectory design is successful in preparing the tooth by conserving the original contour and the clinical design considerations.

Teleoperation control in vitreoretinal surgery demands high precision and swift response. The unique environment of constrained task space yields to the issue of operation method to control the tool tip. In this study, we study two control methods for teleoperation vitreoretinal surgery in a virtual reality (VR) simulated environment with a surgical cockpit, master control arm and Oculus Rift S head mount. System is programed via Microsoft C#, Blender, Unity and Chai3D. The impact on performance with different scaling factors is studied as well to investigate the optimal parameter setting for vitreoretinal surgical teleoperation control.

All the results in this dissertation are verified in simulations and experiments. The methodology, experiment equipment, data and observations from the experiment can be utilized in the development or as inspiration of the future investigation.

The dissertation of Haoran Wang is approved.

Eric C. Sung

Tsu-Chin Tsao

Dennis W. Hong

Jacob Rosen, Committee Chair

University of California, Los Angeles

2022

This dissertation is dedicated to my beloved family and friends.

Table of Contents

List of Figures

List of Tables

List of Symbols

e	tracking error
f	contact force measurement
F_r	reference force
I_x	principal x axis
I_y	principal y axis
I_z	principal z axis
k_d	differential gain
k_i	integral gain
k_p	proportional gain
k_v	virtual stiffness
M	switching gain
p_x	manipulator Cartesian space position in x
p_y	manipulator Cartesian space position in y
p_z	manipulator Cartesian space position in z
R	insertion
v	velocity
x	Cartesian space position measurement
x_r	reference position
x_t	trajectory position

Greek Symbols

α	scaling factor
ε_f	enabling threshold force
ε_x	enabling threshold position
Φ	pitch angle
θ	axial wall taper angle
θ_{bur}	taper angle of the bur
σ	sliding manifold
ϕ	projection angle
Ψ	yaw angle
ψ	axial angle

Acronyms

CAD	computer aided design
CAM	computer aided manufacturing
CBCT	cone-beam computed tomography
CMM	coordinate-measuring machine
DOF	degree of freedom
FDA	US Food and Drug Administration
FSM	finite state machine
ISO	International Organization for Standardization
pHRI	physical human-robot interaction
PVC	polyvinyl chloride
SMASC	sliding mode admittance switching control
SMC	sliding mode control
TCP	transmission control protocol
VR	virtual reality

Acknowledgments

I would like to express my gratitude to all the wonderful people that helped me with this research and everything related to the achievements in my PhD career. Special thanks to my advisor, Prof. Jacob Rosen, who has been supporting me with his unparalleled expertise, vision and patience through years. It is his guidance that helps me break through the hardship during my time of confusion and eventually enters the field of leading research of technology. In addition to that I would like to thank Prof. Eric C. Sung, Prof. Tsu-Chin Tsao and Prof. Dennis W. Hong for their support and advice for the research, and in memory of Prof. Warren S. Grundfest, who was on my committee and helped me with his kind advice. I own thanks to the members of Bionics Lab at UCLA: Ji Ma, Peter Ferguson, Hao Lee, Erik Kramer, Seungmin Jung, Jianwei Sun, Te-Kang Chao, as well as members of IRISS lab who helped me with the experiments with the eye surgery simulator. I also wish to thank my parents, other family members and my friends who have been supporting my decisions, good or bad, and for that I am never alone in my pilgrimage to the temple of science. There are so many words I would like to share, but all in all I am simply blessed by the fact that all the years of effort eventually turn into a tiny stone that could help pave the road to the future.

Vita

2013 - 2022	Graduate Student Researcher, Mechanical and Aerospace Engineering Department, UCLA.
2011 - 2013	Master of Science in Mechanical Engineering, University of Southern California.
2006 - 2010	Bachelor of Engineering in Mechanical Engineering, Qingdao Technological University, China

Publications

H. Wang, J. Rosen, E. Sung. "Automate dental implant surgery system." In preparation.

H. Wang, J. Ma, J. Rosen. "Trajectory design of automated tooth preparation for crowning." In preparation.

H. Wang, M. Rodriguez, J. Ma, J. Rosen. "A study of teleoperation method in virtual eye surgery environment." In preparation.

Chapter 1

Introduction

Robotic technology has been entering the clinics since the last few decades, the main applications involve image processing, computer aided design (CAD), computer aided manufacturing (CAM), haptics and teleoperations. Most applications take advantage of robot's accuracy and manipulability to boost the quality and efficiency in diagnosis or operations. However, automated surgery is still limited in the stage of experiments due to the design complexity in various tasks and the considerations of physical human-robot interaction (pHRI) with respect to safety. Therefore, this dissertation targets the dental and eye surgery application in dental implant, tooth preparation for crowning, and teleoperation of eye surgical tasks to investigate the performance of potential automation or semi-automation of the surgery in a clinical environment.

This chapter introduces the motivation of this dissertation by providing an overview of current status of automation in dental and eye surgery clinics and the advantage of automation for developing design targets of each application. Section 1.1 introduces the current applications and advantages in dental implant surgery. Section 1.2 discusses application of sliding mode control (SMC) in pHRI. Section 1.3 shows the existing and potential applications in tooth preparation for crowning. Section 1.4 shows the current status of the eye surgery. Section 1.5 lists the objects of the study and Section 1.6 overviews this dissertation chapter by chapter.

1.1. Robotics in dental implant surgery

Robotic technology has surged into operating rooms including dental implant surgery (fig. 1.1) within the past decades. Pioneer studies have evaluated precision of robotic dental drilling [1]–[4]. Sun

et al. developed an image-guided surgery system [5]. In 2017, the world's first case of autonomous dental implant surgery was reported [6]. The advancing frontier of technology has been expanding the role that robotic systems can play. However, while robot-assisted surgery is becoming the new reality, such a role inevitably raises concern for contact between human and robot. Physical human-robot interaction (pHRI) has been an extensive issue regarding the automation industry as well as robotic surgery in terms of general protocol, system structure and controller design [7]–[10]. ISO 10218 [11], [12] sets safety standards for industrial manipulators and ISO 14971 [13] specifies risk management principles in medical devices. Due to the unique clinic environment such as local anesthesia and laborious actions, pHRI-based inspection and design adjustment in a dental implant surgery is necessary for robotic surgery system in high level of automation. However, contact control is complicated in such an environment and various behaviors involving position and force tracking can be desired during a surgical drilling process. Real-time switching is demanded in handling contact with uncertainty such as collision [14]–[16], which proposes the challenge of high robustness during the entire drilling task.

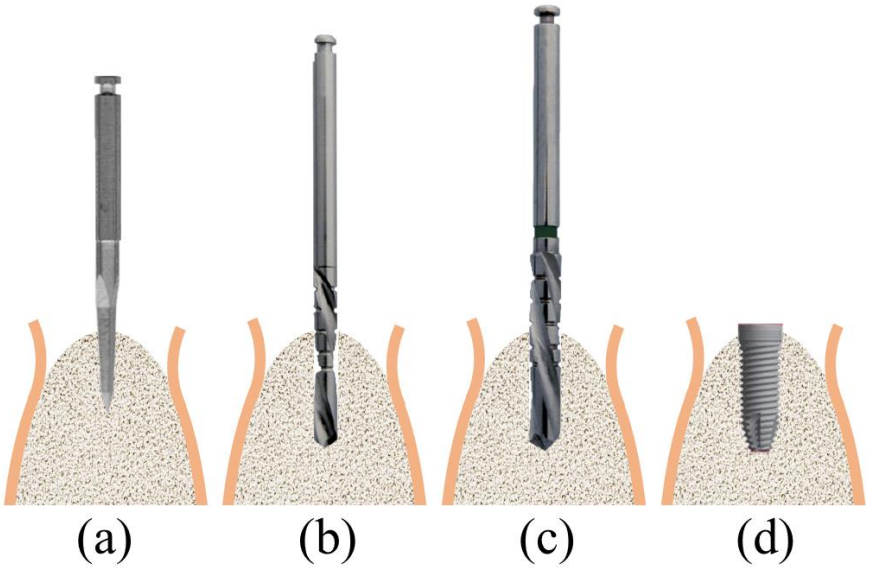

Figure 1.1. Dental implant drilling surgery: (a), (b) and (c) are pilot drilling with different size of bur, (d) is insertion of the implant

1.2. Sliding mode control

Sliding Mode Control (SMC) is a popular non-linear control strategy that has been proven robust against uncertainties and disturbances [17]–[20]. Utkin and Shi [21] generalized the integral sliding mode and its robustness is further examined by Castanos and Fridman [22]. Integral SMC is regarded as a promising solution for controlling admittance [23]–[25]. Li et al. developed a one degree of freedom position/torque switching control with SMC for collision safety [26], yet a system further relevant to the clinical environment is required for a specific surgery. In this study, we propose an SMC control with an admittance sliding surface that can switch tracking control of position/force in real time for an automated dental implant surgery. The controller can track not only the target trajectory with capability of protecting the patient upon unexpected collision but also the reference

force along the drilling direction. The switching is prompt among the distinct behaviors within a short and stable transition period.

1.3. Robotics in tooth preparation

Tooth preparation involves careful design based on principles of the crowning [27]. Dentists must use the bur driven by high speed air turbine to remove part of enamel or dentin following the treatment plan. The quality of the crowning process depends on a variety of factors such as design of the preparation, risk in endodontics or human factors in posture and labor [28-30]. Robotics technology with the advantage of high accuracy and repeatability, has a significant potential in improving the quality of conventional tooth preparation. Since the last decade, CBCT scan has been proved reliable in diagnostics [31] and the imagine guided system has been proposed and tested in clinical relevance with crowning and laminate veneer [32-34]. Imagine processing and CAD/CAM enables the dentists to run diagnosis with a fast and accurate fashion. However, the study in robot systems for automating tooth preparation process with clinical validation is still largely absent or very limited [35]. Fusong and Peijing reported a tooth preparation robot system with superior accuracy and efficiency to manual surgery [36]. Jingang et al. proposed a robot system for automating trajectory with augmented reality [37]. In general, the restrictions for robotic technology to be commercialized in automating the cutting process can involve considerations not only in accuracy and efficiency but in physical human robot interaction (pHRI) as well. The pHRI concerns the contact safety between surgical robot and human operators including the surgeons and the patient within its working range. Such concerns can be addressed with upper level design of a robot system in functions, as well as in trajectory design of the cutting path.

1.4. Robotics in eye surgery

Vitreoretinal Surgery requires extreme surgeon dexterities and precision, while working in a tightly constrained space. These characteristics make the latter one of the most complex types of surgeries in Ophthalmology. Potentially hampering human imperfections have led the way for the implementation of robotic assistance in various surgical fields, with the purpose of maximizing surgical precision, while retaining utmost safety. The efficiency and safety of Robotic surgical platforms have been the focus of study of a wide range of specialties over the past two decades. However, vitreoretinal microsurgery still poses a challenge for various reasons: the small size of the working space; the delicate nature of the tissues involved (retina, optic nerve, vasculature) and the size of some of the retinal structures that are manipulated (the diameter of the largest retinal veins are approximately 150 microns[38] [39]); difficulties regarding spatial resolution, depth perception and plane recognition[40]; the need for optimal visualization; the need to provide the most minimally invasive approach possible; the lack of sufficient tactile feedback[41] [42]; the adversity of overcoming physiological hand tremor[43]; These are all aspects of vitreoretinal surgery that could adversely affect the accuracy and speed of the procedures. Robotic- assisted platforms have already successfully approached some of these issues, in particular, canceling hand tremor and improving surgical precision when compared to manual surgery [44-46].

The da Vinci Surgical System (Intuitive Surgical, Inc, Sunnyvale, CA) is still the most prevalent commercialized FDA approved teleoperated surgical robotic platform for various specialties since its introduction in 1999. The da Vinci System has been applied to the field of Ophthalmology to perform extraocular and intraocular anterior and posterior segment procedures such as corneal laceration repair, penetrating keratoplasty, creation of a continuous capsulorhexis and pars plana vitrectomy [47-50]. Hubschman and colleagues assessed the feasibility of the da Vinci Surgical System for performing

intraocular robotic surgery and addressed the limitations this system presents in terms of visualization, control and maneuverability [51]. In an attempt to further improve robotics knowledge in the field of Ophthalmology Hubschman and colleagues developed the intraocular robotic interventional surgical system (IRISS) which is also an example of teleoperated robotic surgery, dedicated to performing anterior and posterior segment intraocular surgery [52].

1.5. Objectives of the study

There are separate main purposes for each of the three applications. For dental implant surgery the automation relies on the systematic design of automating the drilling process. For tooth preparation the automation requires a proper path for cutting along an irregular surface. For eye surgery the performance of teleoperation demands the investigation of the control settings. The three topics are of author's interest and therefore the purpose of this dissertation are:

- Investigate the systematic design of dental implant surgery and setup a prototype demonstration.
- Study the trajectory design in automating the tooth preparation process for crowning.
- Study the teleoperation control performance in eye surgery.

1.6. Overview of dissertation

In this dissertation, Chapter 2 presents the design of an automated dental implant surgery system. The system takes the pHRI considerations and involves the patient as part of the system interaction. To let the system interact with the patient upon surgery while still being able to protect the patient, I studied the logic of the surgeon during the implant surgery process and designed a final state machine

(FSM) to mimic the human surgeon's decision. I also proposed a simple but effective identification method for the system to identify the current status. I designed a real time control algorithm thus the system can switch between various states tracking position or force. In addition, a prototype surgery demonstration is setup and tested.

Chapter 3 shows the problem of designing a trajectory according to the scanned tooth for crowning. I designed the trajectory path for axial and occlusal trajectory. I proposed two different methods for occlusal surface reduction. An experiment environment is then setup and the trajectories are verified by cutting the 3D printed models.

In Chapter 4, I conducted a simulation study on teleoperation control with a virtual reality simulation environment with different control methods and different control settings. Multiple test subjects perform the tasks and the data is collected and analyzed.

Chapter 5 concludes all the studies in this dissertation and summarizes the results obtained from the three research topics. Future efforts will focus on extending the functions of automation to a high level of the system design.

Chapter 2

Automated dental implant surgery system

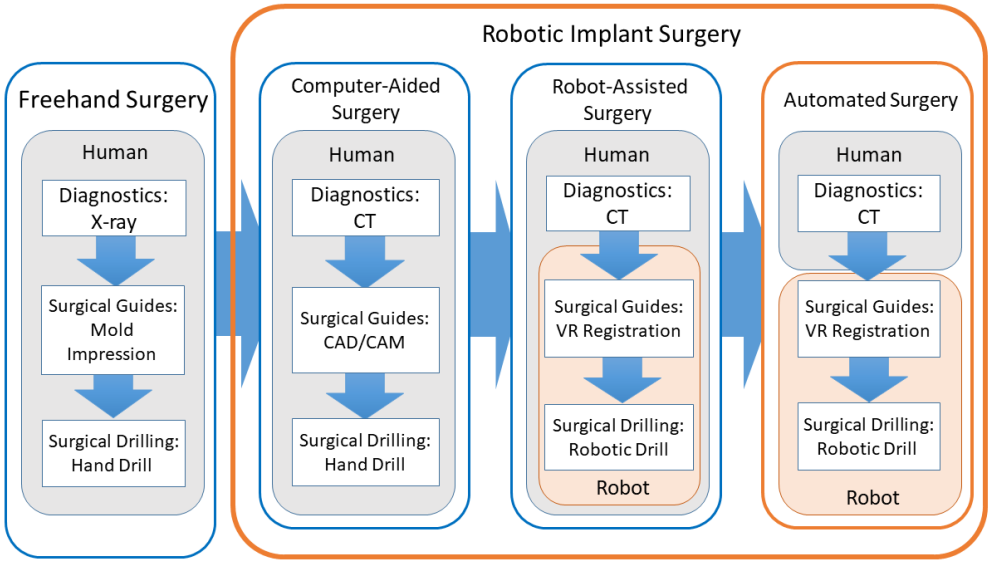

Figure 2.1. Robotics in Dental Implant Surgery.

High	10	The computer decides everything, acts autonomously, ignores the human	
	9	Informs the human only if it, the computer, decides to	Automated Surgery
	8	Informs the human only if asked, or	
	7	Executes automatically, then necessarily informs the human, and	Robot-Assisted Surgery
	6	Allows the human a restricted time to veto before automatic execution, or	
	5	Executes that suggestion if the human approves, or	
	4	Suggests one alternative	Computer-Aided Surgery
	3	Narrows the selection down to a few, or	
	2	The computer offers a complete set of decision/action alternatives, or	
Low	1	The computer offers no assistance	Freehand Surgery

Figure 2.2. Levels of Automation.

The goal of system design presents three major challenges: accuracy, efficiency and safety. Although the requirement of accuracy can be fulfilled by modern industrial manipulators, achieving efficiency and safety involves perceptions of interaction between surgeons and patients in the clinical environment. Fig. 2.1 shows the idea of an automated surgery system in dental implant surgery and fig. 2.2 shows the corresponding level of automation based on Parasuraman and Sheridan [53]. To achieve the goals in a higher level of automation, we propose the structure of the system as shown in Fig 2(a). The three entities of surgeon, patient and robot will interact with each other. Human surgeon will prepare the surgery by planning the trajectory with CBCT scan and CAD software, and will monitor the surgery. The automated surgery system will perform implant drilling task. Patient status identification monitors patient motion and feeds current status back for AI surgical decision. AI surgical decision connects upper level trajectory control to base level motion control. The decision that either the system should press on the surgery or protect the patient will be executed by real-time control algorithm as core of the lower level structure in the drilling task.

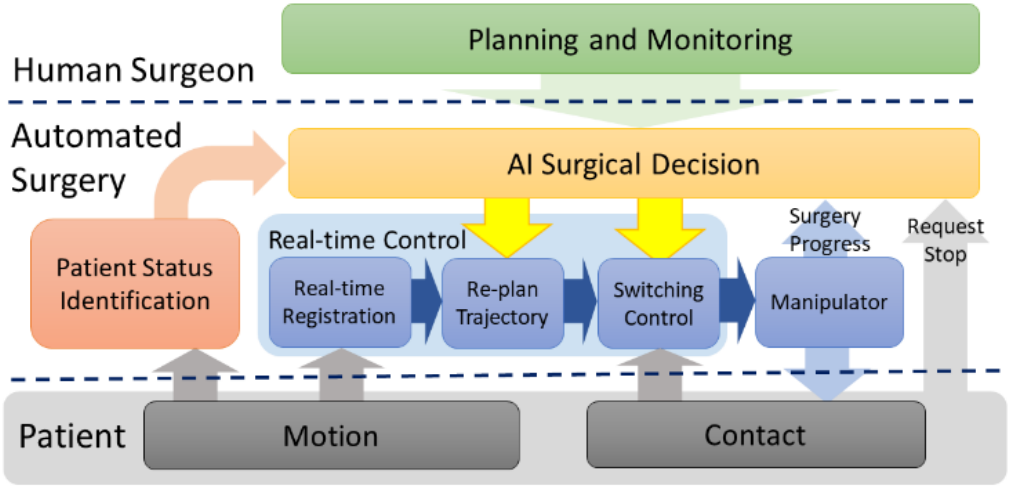

Figure 2.3. System structure.

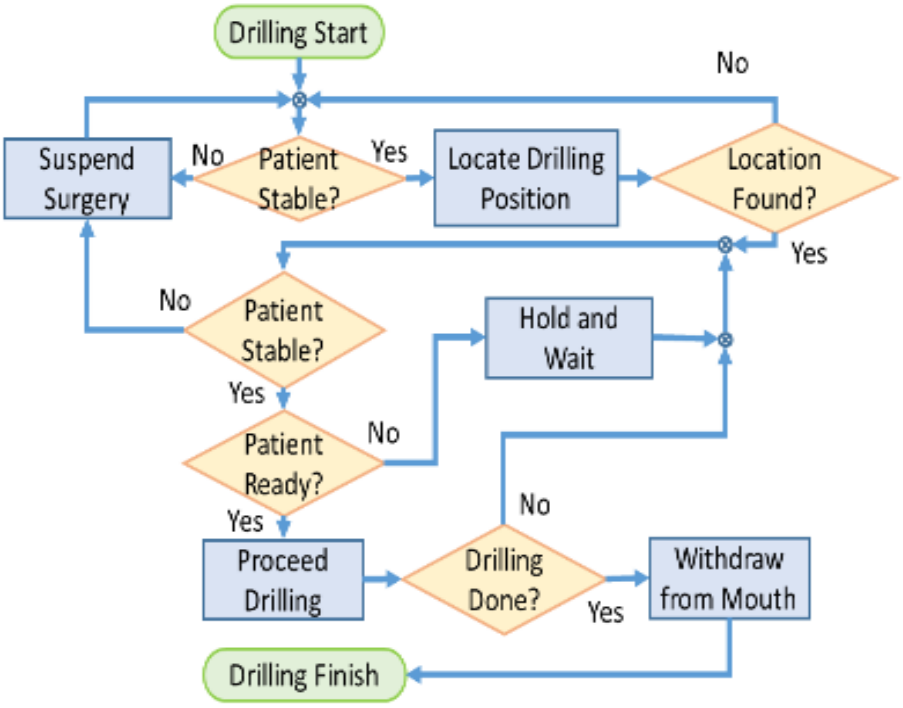

Figure 2.4. Human Surgeon Logic Flow Chart: Actions of "Locate Drilling", "Hold and Wait", "Withdraw from Mouth" requires compliant position control. Action of "Proceed Drilling" requires contact control from the surgeon's hand. Action of "Suspend Surgery" requires protective behavior of unconditional yield upon contact. "Patient Ready" indicates the patient's motion is trivial and it is safe to proceed drilling. "Patient Stable" indicates the patient's motion is not suitable for drilling but the situation is under control.

The structure underlines the interaction between the automated system and the patient. During the surgery, if proper conditions are satisfied, the automated system should push on with the surgery. However, upon unpredictable or untraceable motion, the automated system should pause the surgery and focus on protection of the patient. Therefore, the design of the automated system calls for an analysis of human surgeon's behavior during the implant drilling task. The logic flow chart of a human surgeon performing implant drilling process is shown in fig 2.4. There are three elements in the chart

that correspond to the three fundamental problems in the system structure. The first element is the decision block that identifies the patient status as ready (good to proceed with drilling), stable (not ready but system can predict and track patient motion), or unstable (system cannot track patient motion). The second element is the flow line that makes decisions of the surgery and the third element is the process block that performs real time control. Therefore, patient status identification, AI surgical decision and control algorithm are designed for the automated surgery system.

2.1. Methodology

2.1.1. Patient status identification

Automation of this robot system depends on a logic input of the patient in order to assess current patient status, therefore we need to convert numerical measurement into a logic signal that classifies a patient motion into three categories: ready, stable or unstable. The status of ready indicates that the patient is in minor motion and ready for drilling operations. The status of stable indicates that the patient is not ready due to certain motion but everything is still within control of the surgeon. The status of unstable indicates that the patient is involved with a major motion such that the surgery needs an emergency stop. In robot system, we define a "ready" status of a patient as the motion does not impact robotic drilling accuracy, the "stable" status of a patient as when the patient is in minor motions that can be tracked by robot system but cannot guarantee a high precision drilling, and the "unstable" status of a patient as when the patient is in major motions that either cannot be tracked or will cause critical damage upon collision. Even though the odd of having a patient panicking during the surgery is relatively low, the robot will nevertheless be responsible for detecting potential instability and preparing safety protection.

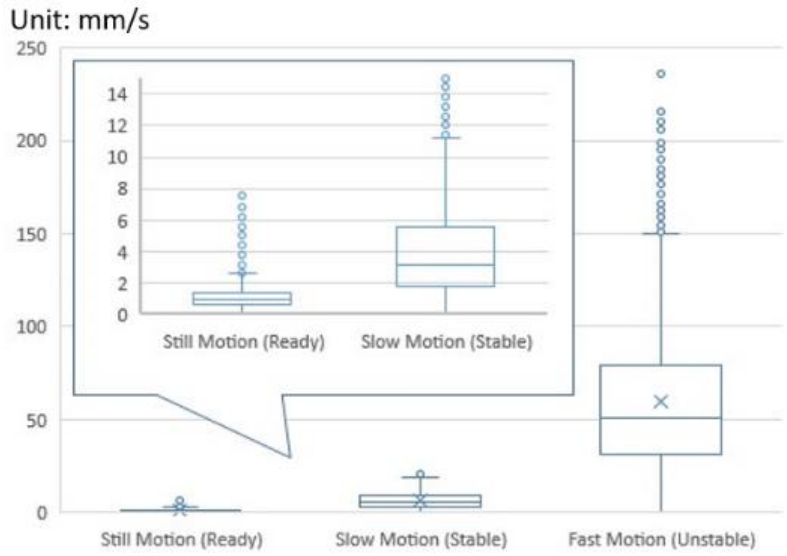

(a)

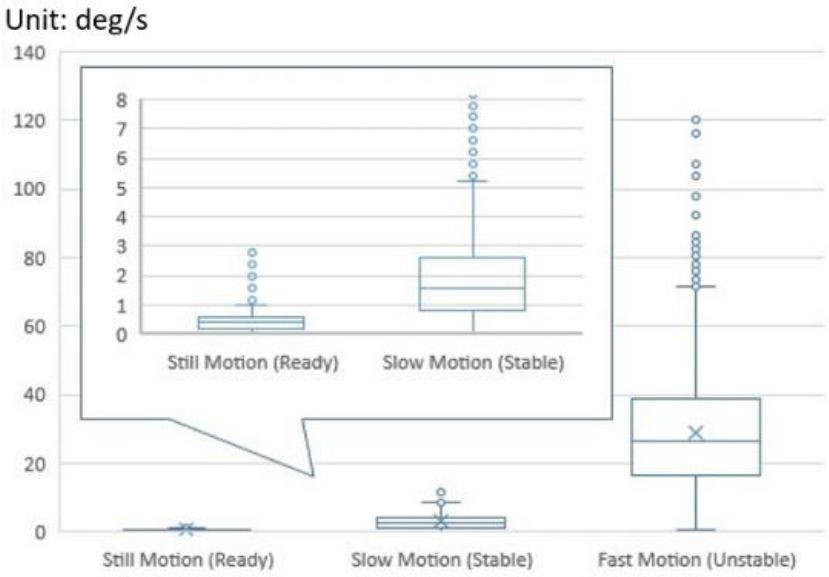

(b)

Figure 2.5. Preliminary test for patient motion: (a) data distribution of linear velocity for different patient status, (b) data distribution of angular velocity for different patient status

The proposed method to identify patient status in this study is to classify motion in real time based on the patient's position measurement. Therefore, a preliminary experiment is conducted to investigate feasibility of such mappings. The test subject bites a teeth cast mold and lies in a surgical position. The cast mold is connected to an MX Digitizer as coordinate measuring machine (CMM) to measure position and rotation with respect to the digitizer's base frame (Fig. 2.5). The base frame is then converted into the patient's mouth center by transformation matrices. Linear and angular velocity is calculated to indicate patient's motion for analysis. The test subject performs typical action of "ready", "stable" and "unstable" motions and the position data in 6 degree of freedoms for each motion is recorded. The "ready" motion requires test subject to remain still and calm as possible for an ordinary drilling. The "stable" motion requires test subject to perform a slow and gentle motions such as slowly turning the head or swallowing, which would usually cause the surgeon to hold current operation without having to suspend it. The "unstable" motion requires test subject to perform relative drastic motions such as tremoring and sudden head shaking, which will force an emergency stop of the operation. Linear and angular velocity is calculated based on the measurement. At one sampling time only the maximum among the three directions of linear velocities and the maximum among the three directions of angular velocities are used to check for the threshold values. A statistical result is shown in fig. The sampled data of the linear and angular velocity between "ready" and "stable", "stable" and "unstable" indicates a weighted distribution pattern for three statuses, therefore it is possible to classify the motion by monitoring patient motion with velocity threshold. There are two thresholds for the classifier, one is to classify between "ready" and "stable" and the other between "stable" and "unstable". The threshold between "ready" and "stable" depends on the capability of robot performance as the primary concern is the accuracy of robotic drilling under small position tracking perturbation. The threshold between "stable" and "unstable", however, depends on the

motion patterns of human since the primary concern is the protection of the patient. Although the preliminary test result indicates a clear divergence, we expect monitoring threshold velocity as a sub-optimal solution of the problem as it ignores the continuity of human body motion and variety of habitual individual behaviors.

The transition from "ready" to "stable/unstable" and "stable" to "unstable" is instant, however, to prevent frequent change of robot behaviors, the transitioning into "stable" status will cause a small period of holding time before it can transition back to "ready". Transitioning into "unstable" should put the system into a standby passive mode such that the status will remain as "unstable" until the surgeon has the problem cleared and performs a manual reset.

2.1.2. AI surgical decision

A finite state machine (FSM) is deployed to model the logic flow of the surgery process. A complete implant drilling process consists of 7 states as shown in fig. 2.6: prepare to enter the mouth (prepare), locate drilling position inside the mouth (approach), proceed drilling operation (engage), stop or finish drilling (disengage), pull out from the mouth (detach), resume to home position (wind-up), suspend surgery at current position (passive). 7 frames are defined for trajectory design of the 7 states. {D} is the fixed manipulator base frame. {H} is the default home position. {Tip} is the drill tip frame. {M} is a fixed CMM base frame. {L} frame is the implant drilling start position that can be defined in pre-surgery plan and calibrated before surgery starts. {W} and {S} are a working frame and a safe frame defined inside and outside the patient mouth with respect to {L}. Once {L} is calibrated, CMM will measure {L} as the patient's motion and the manipulator will measure {Tip} as tooltip position. (Fig. 2.7) Further details can be found in the following state transition design.

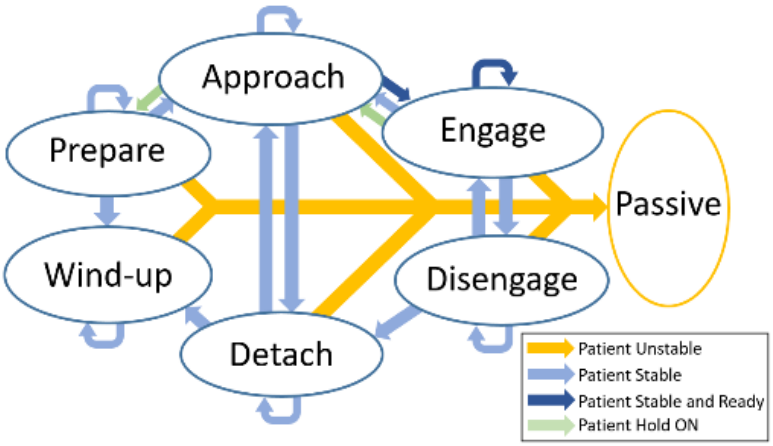

Figure 2.6. Finite state machine model.

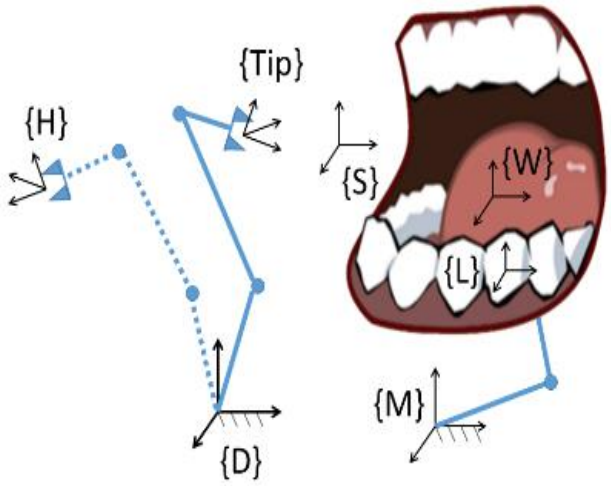

Figure 2.7. Frame definition.

Fig. 2.8 shows state transition for FSM model. Input of "current trajectory" and "drilling done" measures progress in current state. If FSM maintains the current state after progress is finished, the trajectory will be held at the target position. Input of "patient ready", "patient stable" and "patient unstable" measures current status of patient as classification result of patient status identification. FSM will not only switch surgical actions by operation progress but patient's intention as well. In addition to detecting the patient's intention by passively monitoring the motion, we introduce one more input

of "patient interruption" that allows the patient to actively interrupt current operations on demand. Upon "patient's interruption" is triggered by patient during the surgery, input signal of "patient ready" and "patient stable" will be overwritten and robot system will try to pull the bur out from patient's mouth and wait for patient to release interruption status before resuming to the surgery. In summary, FSM will switch among 7 states based on 3 input signals: if current action is completed; if the surgery is completed; and intention of the patient.

States	Current Trajectory	Drilling Done	Patient Ready	Patient Stable	Patient Unstable	Patient Hold ON
Prepare	From {H} to {S}	Yes	Wind-up	Wind-up	Passive	Wind-up
		No	Prepare	Prepare	Passive	Prepare
	Arriving at {S}	Yes	Wind-up	Wind-up	Passive	Wind-up
		No	Approach	Approach	Passive	Prepare
Approach	From {S} to {W}	Yes	Detach	Detach	Passive	Detach
		No	Approach	Approach	Passive	Detach
	Arriving at {W}	Yes	Detach	Detach	Passive	Detach
		No	Engage	Approach	Passive	Detach
Engage	From {W} to {L}	Yes	Disengage	Disengage	Passive	Disengage
		No	Engage	Disengage	Passive	Disengage
	Arriving at {L}	Yes	Disengage	Disengage	Passive	Disengage
		No	Engage	Disengage	Passive	Disengage
Disengage	From {L} to {W}	Yes	Disengage	Disengage	Passive	Disengage
		No	Engage	Disengage	Passive	Disengage
	Arriving at {W}	Yes	Detach	Detach	Passive	Detach
		No	Engage	Disengage	Passive	Detach
Detach	From {W} to {S}	Yes	Detach	Detach	Passive	Detach
		No	Approach	Approach	Passive	Detach
	Arriving at {S}	Yes	Wind-up	Wind-up	Passive	Wind-up
		No	Approach	Approach	Passive	Detach
Wind-up	From {S} to {H}	Yes	Wind-up	Wind-up	Passive	Wind-up
		No	Prepare	Prepare	Passive	Prepare
	Arriving at {H}	Yes	Wind-up	Wind-up	Passive	Wind-up
		No	Prepare	Prepare	Passive	Prepare
Passive	{Tip}	Yes	Passive	Passive	Passive	Passive
		No	Passive	Passive	Passive	Passive

Clinical Relevance	Proceed normally with surgical operations
	Hold operations and wait for patient to get ready
	Patient ready, resume to the previous surgical operation
	Suspend surgery and wait for surgeon to manual rest (highest order)
	Wait for patient to manual release hold (second highest order)
	Not applicable in a normal surgery process

Figure 2.8. Finite state machine switching chart.

The state of "prepare" requires tracking a safety position {S} outside the patient's mouth which is the process of establishing real-time registration of the patient from the robot base frame. The robot manipulator has a relatively open workspace thus instead of pursuing accuracy the primary objective

is to reach target position and watch out for any contact. Physical HRI demands that the robot system must follow a safety regulation of maximum velocity during automation within contact range of human. However, with sufficient safe clearance human surgeon will be allowed to manually hold and move the hand piece to accelerate the preparation process. On the other hand, to create a safe clearance for the surgery a human surgeon can also block the robot motion temporarily when emergency break of the entire surgery is not necessary. Upon arriving {S}, the system will switch to the next state of approach unless the patient demands to hold the surgery (patient interruption signal ON), or the system identifies an unstable patient motion. Other state transitions are unlikely to happen in a normal surgery and are designed only for algorithmic stability.

The state of "approach" drives the robot system in an attempt to enter the patient's mouth towards a surgical preparing position {W} in the center of the oral cavity. An explicit reference trajectory is required to avoid collision on lips, teeth, tongue, etc. Robotic tool must follow the real-time registered reference trajectory and based on pHRI principle we propose an additional protective measure which is being able to react and yield to any unexpected contact while tracking the reference trajectory. The system will keep approaching as long as it can maintain a safe tracking of the patient's motion. Upon arriving {W}, the system will wait for the patient's status to become ready before commencing the surgical operations. If the patient sends an interruption signal to demand the surgery to be held, states will be transited to detach in an attempt to pull handpiece out of the mouth. If unstable patient motion is detected, surgery will be switched to passive as an emergency break. Other state transitions are unlikely to happen in a normal surgery and are designed only for algorithmic stability.

The state of "engage" is the process of surgical drilling that consists of two phases. Phase one is to reach target drilling position {L} following a pre-designed trajectory and second phase is to commence drilling operations at {L}. Phase one requires accurate position tracking of {L} as well as

safe measure similar to the state of "approach", while phase two is designed as a force tracking control task. Both phases demand that the patient must be very stationary (patient status identified as ready). Otherwise states will be transited into disengage and the drilling bit will be retreating to the surgical preparing position {W} until the patient is ready again. Once drilling depth measurement indicates the drilling is done, state will be switched to disengage. If the patient sends an interruption signal to demand the surgery to be held, states will be transited to disengage to retreat the bur to {W} before attempting to pull the handpiece out of the mouth. If an unstable patient motion is detected, surgery will be switched to passive as an emergency break. Other state transitions are unlikely to happen in a normal surgery and are designed only for algorithmic stability.

The state of "disengage" will retreat the bur to {W} following a pre-planned trajectory in real-time registration. This state is either a safe measure to wait for the patient with trackable but too much motion to stabilize for drilling, or transitioning state before pulling out the bur from the mouth (state of detach) when drilling is done or the patient demands an interruption of the surgery. Unstable patient with un-trackable motion will trigger the passive state as an emergency break.

The state of "detach" will try to pull out the bur from the patient's mouth following the pre-planned trajectory with real-time registration, usually the reverse path for approach state. Physical HRI principle demands protective behavior upon unexpected contact. Other state transitions are unlikely to happen in a normal surgery and are designed only for algorithmic stability.

The state of "wind-up" will reset the robot arm to its home position. As a reverse state of "prepare", the task of wind-up has the same property and requires protective behavior as well upon unexpected contact, and the handpiece can also be manually held and moved at the surgeon's convenience.

The state of "passive" set system in a pure protective status. The system will abort all current tasks or tracking but leave the bur at where the state is triggered. The bur is subject to any contact without resuming to its original position. In this state, the patient or surgeon can push the robot arm away to avoid further danger. The entire surgery will be suspended until the emergency is cleared and the surgeon reset the system to home position to restart the surgery.

2.1.3. Control algorithm

Based on patient status during each of the states, the FSM will switch states for various behaviors. With concerns of safety interaction, the tasks can be sorted into three categories according to controller tracking targets for the behaviors. The states of preparation, approach, engage (reaching target frame {L}), disengage, detach and wind-up requires the controller to track a desired trajectory. The robot needs to yield upon any unexpected contact during trajectory tracking, i.e. the controller should be able to control contact admittance as a force disturbance during trajectory tracking. The state of engage (commence drilling at {L}) requires the controller to maintain a certain level of contact. As bone density can be various for the patients, tracking a desired drilling thrust force is preferred than tracking a constant feeding rate for a better chance to avoid excessive friction, which can overheat bone issue and cause implant failure such as cracking. The state of passive requires the controller to instead yield to any contact and attempt to follow the contact for protection purposes. The three control tasks with their control targets are listed in Table 2.1.

Table 2.1. Breaking down from surgical targets to controller design.

Surgical Tasks	Control Targets	Controller States

Locate drilling position, Hold current position, withdraw from mouth	Track reference position; compliant behavior	Trajectory Tracking Mode
Surgical drilling	Track reference contact force on drilling direction	Force Tracking Mode
Suspend surgery and avoid contact for safety	Track reference force as 0	Passive Mode
Decision making	Change control gains and tracking errors	Mode Switching

Though the three control tasks can each be independently achieved by a conventional PID admittance control law, the real time switching among trajectory tracking, drilling thrust force tracking and contact avoidance poses a problem. As the three control tasks have fundamentally distinct nature, the control gains span in a large range and the structures are also incompatible. The trajectory tracking task demands a PD dominating control with a trajectory tracking signal for a swift response. The drilling thrust force tracking demands a double integral term in order to track a force signal in drilling dynamics. The passive contact avoidance task demands a PI dominating control. Switching control signal parallel among the 3 distinct control laws would cause large overshoot or long transient periods. Therefore, in the original admittance control scheme we replace the PID admittance dynamics with sliding mode dynamics in order to take advantage of continuous convergence during real-time task switching. We refer to this control law as a Sliding Mode Admittance Switching Control (SMASC).

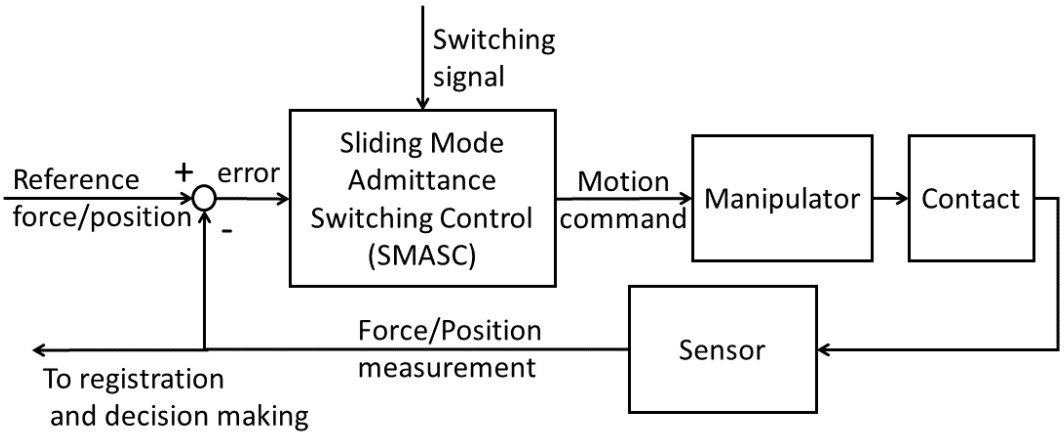

Figure 2.9. Control block diagram.

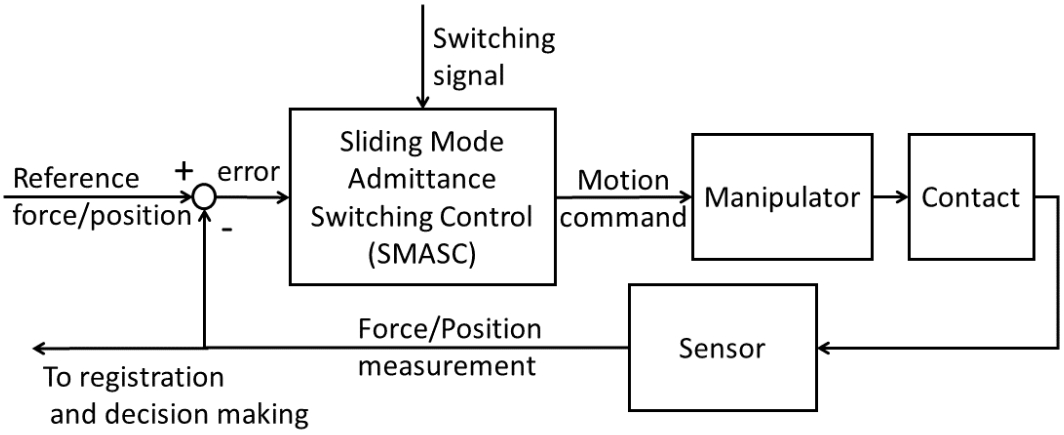

Figure 2.10. Structure of SMASC block.

The control scheme is shown in fig 2.9 and fig 2.10. The sliding surface for SMASC in a dental implant drilling dynamics is defined by

$$\sigma = k_p e + k_i \int e dt - k_d \ddot{x} \tag{1}$$

where k_p, k_i and k_d are parameters of sliding surface representing proportional, integral and derivative terms similar to a mechanical admittance of $Y(s) = V(s)/F(s)$. The parameters in the sliding surface need to be tuned and do not represent the actual mechanical admittance for the contact. The term $-k_d \ddot{x}$ is to replace $-k_d \dot{e}$ to avoid differentiating the noised force measurement. Note that the contact dynamics for "trajectory tracking mode" and "passive mode" is modeled to be linear elastic and in that sense we should have set $\dot{e} \propto -\dot{x}$, however, by linearizing the industrial manipulator as a 2nd order system, the convergence of a velocity sliding surface requires a relative degree of 3 rather than 2. Therefore, we replace $-k_d \dot{x}$ with $-k_d \ddot{x}$ to maintain consistency with "force tracking mode", where $\dot{e} \propto -\ddot{x}$ due to the linearized drilling dynamics between thrusting force and feeding rate [54]. Although by increasing order the sliding surface no longer entirely represents the mechanical admittance during an elastic contact, the convergence of error still serves the same goal. In addition, proportional term is the dominating term in the elastic contact and in force drilling proportional term and integral term are dominating terms, therefore the "admittance switching surface" with modified differentiation term should be capable of performing admittance behavior such as yielding upon contact, which is verified via experiments in later section.

The first order switching control signal on velocity is defined as

$$v = M \cdot sgn(\sigma) \tag{2}$$

and the output of the law is a motion command of trajectory x_t for the manipulator.

$$x_t = x_r + \int v dt \tag{3}$$

In order to enable position or force tracking in this control law, error is defined parallel as $e = F_r - f + k_v(x_r - x)$, where F_r is the reference force, f is contact force measured by the sensor

where dynamics of the sensor structure is ignored, x_r is reference position, x is position measurement and k_v is a parameter representing a coefficient for a "virtual stiffness" term that could drive x towards x_r. When switching system into "trajectory tracking mode", we need to set $F_r = 0$ such that $x \rightarrow x_r$ when $e \rightarrow 0$ if $f = 0$. When there is a contact, f serves as a disturbance such that x_t will be pushed away from x_r. This accomplishes the goal of protective behavior during unexpected contact when locating the bur to the target position. When switching system into "force tracking mode", we need to set $k_v = 0$ when e becomes a force tracking error. When switching system into "passive mode", we set both $F_r = 0$ and $k_v = 0$, in which the system will only yield upon unexpected contact without tracking a reference signal. One known issue for first order sliding is chattering. With large gains we shall expect chattering of velocity v upon convergence. The integral of v in equation (3) can improve the issue of discontinuity as manipulator takes x_t as control output, yet a better performance may be desired for both surgical operations and protective behaviors. Therefore, a classical approach would be to replace sign function with saturation function (Eq. 4). Note that this comes with the cost of reduced range of stabilizing gains, since the convergence of the control law relies on robustness of first order SMC scheme but applying saturation function will weaken the control law's robustness. In a later experiment, we will investigate and verify the performance of stability.

$$v = M \cdot sat(\sigma) \tag{4}$$

2.2. Experimental protocol

2.2.1. Simulation

To investigate potential performance of the control algorithm, a one degree of freedom drilling model is constructed with Matlab Simulink 10.0 by Runge-Kutta method at a fixed step of 0.1 millisecond. An industrial arm is identified as a 2nd order system based on the assumption of decoupled degree of freedoms and workspace far from any singular position. Linearized drilling contact dynamics for cortical layer and marrow are modeled according to preparatory test drilling data of the material. A 0.05 second delay is placed to simulate limited command frequency. Simulation data provides reference in tuning parameters in prototype experiments.

2.2.2. Equipment setup

The system prototype is built around a Denso VM60 industrial arm. Position is measured by the manipulator encoder with repeatability of ±0.07mm, velocity and acceleration signals are calculated by first order differentiation of the position measurement. An ATI mini 40 6-DOF Force/Torque sensor is mounted on the wrist of the arm that measures contact force. Sensor data is acquired by National Instruments NI-DAQmx device and sent to the computer program through a USB port. A Nobel Biocare OsseoSet 200 drilling unit is deployed for the drilling test. The handpiece is mounted on the force sensor via a customized aluminum adaptor. Force measurement is calculated via transformation matrix from sensor base frame to tool tip position. In this experiment, the tool trajectory covers a limited space within 100mm with negligible task space rotation, and robot motion speed is limited below 10 mm/s. Therefore, gravity and inertia caused by the hand piece and adaptors can be compensated by offsetting the force sensor reading. A PVC mandible implant drilling training model which has comparable density of bone tissue is bolted to the stainless steel fixture. The fixture

is bolted to the experiment platform. The controller is programmed in the Microsoft Visual Studio C++ environment based on Denso b-CAP communication protocol at frequency of 20Hz. It sends positioning commands to the Denso manipulator RC-7 controller and receives I/O signals and the encoder position measurement data through TCP connection. The RC-7 controller outputs torque for motor actuation. Fig. 2.11 shows the setup of equipment and software communication.

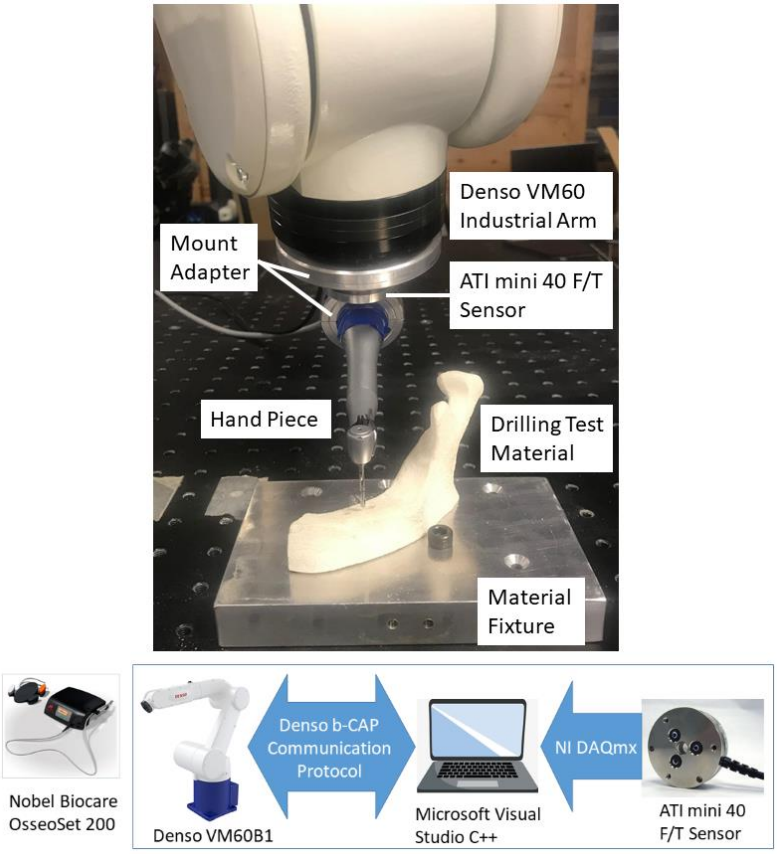

Figure 2.11. Setup of experiment.

2.2.3. Experiment design

A total of 9 scenarios including 3 states and all 6 possible switching transitions are investigated via simulations and experiments. The tasks of 3 states are tested to examine convergence and performance of admittance behavior such as avoiding or tracking contact. The 6 switching tasks are designed

according to each state's scenario with some clinical relevance. Among the 9 sets of experiments, trajectory tracking, switching from trajectory tracking to force tracking and switching between trajectory tracking and passive are designed in 3 DOFs to test response in non-surgical contact, the rest are designed in 1 DOF with force drilling being a major interest. Based on this frame we propose criteria according to clinical experience as shown in Table 2.2.

Table 2.2. Performance Criteria.

	Trajectory Tracking	Force Tracking	Passive
Steady State Error	±1mm (trajectory) ±0.3mm (target position)	±1N	N/A
Rising Time	< 1s	1s	< 1s
Settling Time	1s	3s	1s
Overshoot	No position overshoot	< 3N	No position overshoot
Response upon Contact*	Fast (< 150 mm/s)	Slow (2mm/s)	Very fast (<300mm/s)

*Response speed is based on surgeon's experience

To test performance of "trajectory tracking mode" and "passive mode" subject to contact, we simulate different types of collision potentially caused by jaw moving, finger touching, finger pushing or tongue licking by generating impulse and step perturbations as force disturbance. To achieve a safe pHRI, the controller should not only react within ISO safety standard but the reaction should be comparable within range of estimated motion of a human surgeon as well. To test the robustness of" trajectory tracking mode" upon contact we generate an impulse wave of force disturbance. A step perturbation is generated as well to inspect force-disturbed switching transition behavior between non-force tracking states of trajectory tracking and passive states.

Since contact yielding during trajectory tracking serves as the instant safety protection before system can switch to passive state and pause the surgery, controller can disable virtual stiffness term, which is equivalent to a temporary passive state, in order to provide further protection during non-surgical contact, i.e. $k_v = 0$ when $|f| > \varepsilon_f$, where ε_f is an enabling threshold upon evident contact. It also serves as a force signal filter for measurement noise. Note that disabling virtual stiffness during contact sets the controller to perform as a damper, while enabling virtual stiffness during contact sets the controller to perform as a linear spring. When the system is resuming to reference trajectory after a large contact disturbance, a fast recovery may invoke an overshoot that could cause severe damage. Though we can resolve this issue by tuning the sliding surface gains in equation 1 and trading off part of dynamic response, we propose another solution by taking advantage of SMASC's velocity sliding nature. When the tooltip is close enough to reference trajectory, i.e. $|x_r - x| < \varepsilon_x$, the virtual stiffness term can be disabled by setting $k_v = 0$. However, if system will not respond to contact, i.e. $|f| < \varepsilon_f$, the perturbed trajectory $\int vdt$ need to be gradually reduced to 0 for positioning tracking. In this experiment we multiply $\int vdt$ by a ratio of 0.8 for convergence. Note that disabling virtual stiffness around reference trajectory does not only reduce overshoot during convergence without sacrificing dynamic response but also reduces chattering caused by force sensor noise.

For force drilling, there are three clinical concerns to be addressed: performance, reference and the issue of surface collision. Performance criteria for force tracking is designed as in Table II but unlike trajectory tracking and passive, there exists a clear overall boundary that requires close inspection through experiments. Due to the difference of material impedance for drilling through cortical layer and marrow part of bone tissue [55], for the drilling experiment on bone model we set reference force as 12N to penetrate a 2.5mm hardened surface layer and 5N to complete the remaining depth. The thickness of hardened surface and reference forces can be determined based on pre-surgery

diagnosis of bone tissue. In an admittance model based force tracking, the integral term $\int edt$ that drives reference tracking is sluggish, therefore the drilling bit can "crash" upon the contact surface causing instability. However, this issue can be resolved in SMASC by limiting M to a lower feeding rate when closing to a pre-planned "expected contact surface", and the integral term will be reset upon reaching this surface to avoid large integral of error caused by limited M. The reason for applying a pre-planned surface rather than a real time detected contact surface is that there could exist non-drilling contact such as collision or tongue licking that could disturb contact detection via force sensor. For passive response, we hold the current reference position upon switching signal, therefore the system will not attempt further position tracking.

2.3. Result and discussion

2.3.1. Patient status identification

There are two threshold values that need to be determined through experiment. The threshold between ready and stable status depends on tracking dynamics of the manipulator. Based on the denso VM60 industrial robot arm we use in the prototype system we set the velocity threshold as 3mm/s for linear velocity and 1 deg/s for angular velocity. The threshold between stable and unstable status, however, needs to be determined from the patient's motion data. The velocity data of the patient is grouped into a period of 0.5 second (10 consecutive data each group at 20Hz sampling rate). The grouped data of "stable" and "unstable" is then partitioned into 10 equal sizes of subsets for a 10-fold cross validation. For each fold threshold is determined by maximum magnitude in the "stable" training set. The cross validation result is shown in fig 2.12. The overall score of threshold in 6 degree of freedoms ranges between 0.88 and 1. The maximum mean score of 6 degree of freedoms is 0.9841 where the thresholds are x = 14.4, y = 8.6, z = 19.8, Rx = 7.8, Ry = 6.2, Rz = 7.0 mm/s

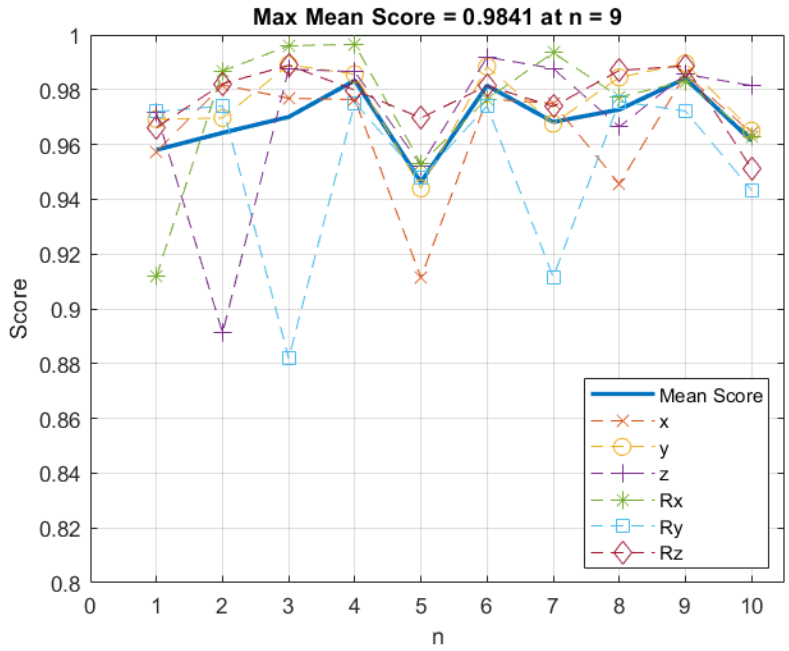

Figure 2.12. Cross validation result for patient status identification.

2.3.2. AI surgical decision

To assess the logic of the FSM AI model, we will trigger each input during every state and check if the system can always converge to a complete drilling process. From the table there are 6 inputs that would affect switching of the states. Trajectory and "drilling done" inputs are part of the FSM model as it is physically inadmissible to have current trajectory jump from {S} to {L} without passing through {W}, or drilling status switched from "drilling complete" to "drilling incomplete" during an ordinary drilling process. The signal of 3 inputs of patient status are objective measurement but the signal of "hold" indicates the subjective intention to interrupt the drilling. When the two signals are triggered at the same time, the unstable status of the patient takes the highest priority in the FSM model as a prompt protection against unexpected motion. Only when status is not unstable will the

system respond to the patient's request to hold and pause. And the system proceeds the surgery at lowest priority when the patient is ready or stable and does not attempt an interruption. Since "patient unstable" will put the system locked in passive mode and instantly stop the automation, we only need to test impact on triggering hold signal or switching patient status between ready and stable.

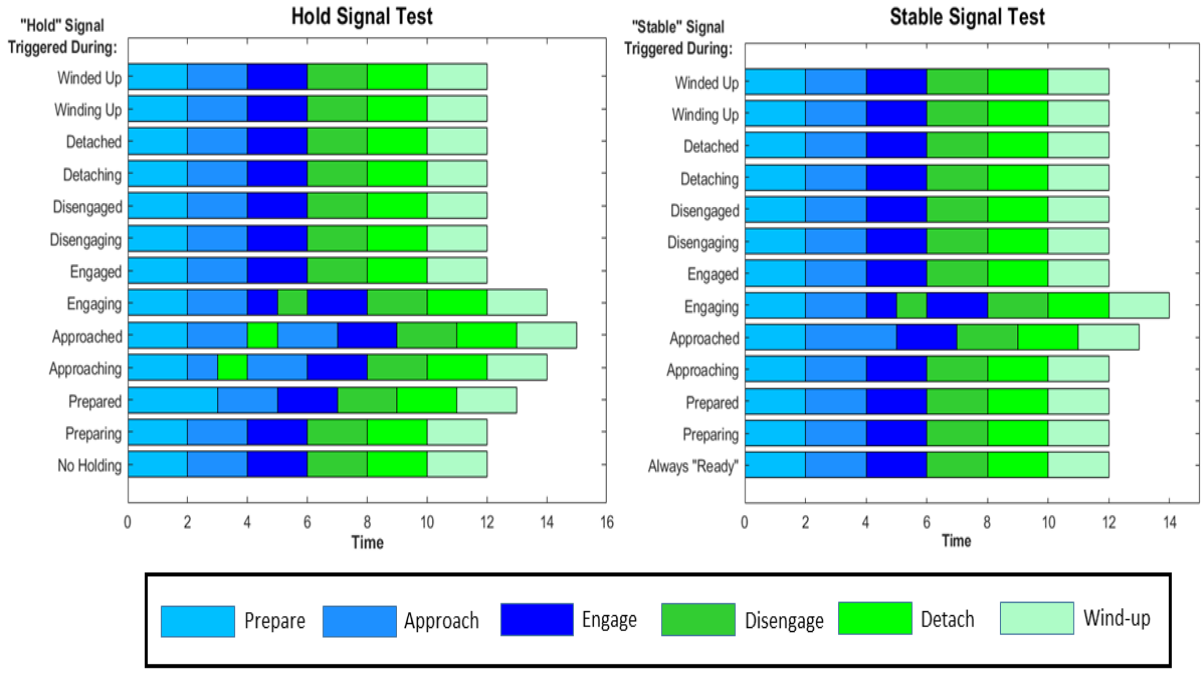

Figure 2.13. Simulation result of AI surgical decision.

The test result is shown in Fig 2.13. The left and right chart indicates triggering "hold" signal and patient status as "stable" during each of the states of the process assuming a default patient status as "ready". It can be seen that the process can always resume to the ordinary drilling process after the patient releases the holding request or becomes ready for the drilling. It also verifies the logic to overwrite "patient stable" signal upon triggering "hold" signal, as a subjective interruption would

suggest pulling the bur out from the mouth and not being ready awhile would simply delay the drilling process.

2.3.3. Control algorithm

Performance for simulation and experiment of "trajectory tracking mode" descending 100mm on z direction (3 DOF trajectory for experiment and 1 DOF for simulation) is shown in Fig 2.14. Perturbations are generated as an impulse of 15N around t=5s, a step of 2N around t=10s, and a 2.5Hz pulse wave of magnitude 15N starting at t=15s. Bounded purple regions of A, B and C indicate estimated ranges of physically admissible response of a human surgeon. Bur starts at t=0s (steady state tracking error tolerance of ±1mm) and converges to the drilling target at t=25s (steady state tracking error tolerance of ±0.3mm). Performance for simulation and experiment of "force tracking mode" is shown in Fig. 2.15. Drilling bur starts around 12mm above contact surface, and switches from tracking a 12N contact force into 5N contact force upon penetrating a 2.5mm cortical layer. Controller response in the experiment is divided in 4 regions. In region A, bur approaches the contact surface with a maximum feeding rate of 3mm/s. In region B, when approaching an expected contact surface, the controller slows down to 1mm/s. In region C, the controller lifts the feeding rate limitation for a 12N contact tracking. In region D, upon a drilling depth of 2.5mm, the controller switches reference force from 12N to 5N for marrow tissue drilling. Region E shows the performance criteria of the force controlled drilling. Performance for simulation and experimentation of "passive mode" is shown in Fig. 2.16. Perturbations to simulate collisions are generated as an impulse of 15N around t=5s and a step of 2N around t=10s. Bounded regions of A and B are references for the common response rate of a human surgeon.

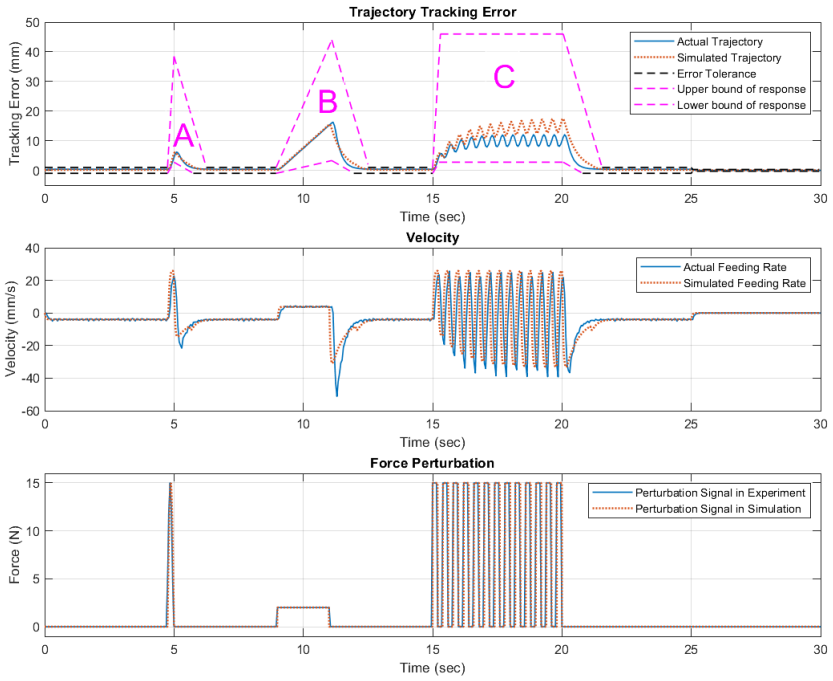

Figure 2.14. Test result for trajectory tracking.

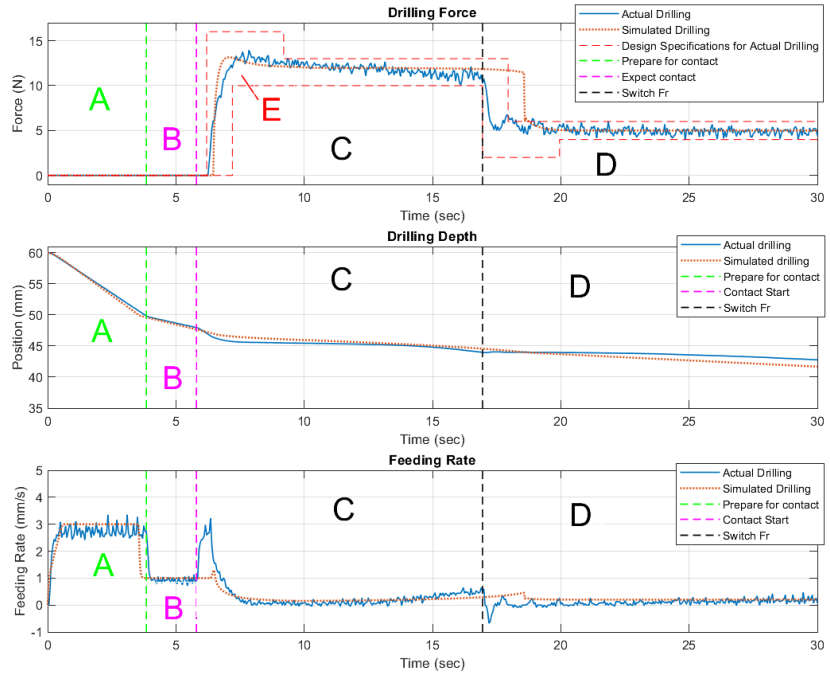

Figure 2.15. Test result for force tracking.

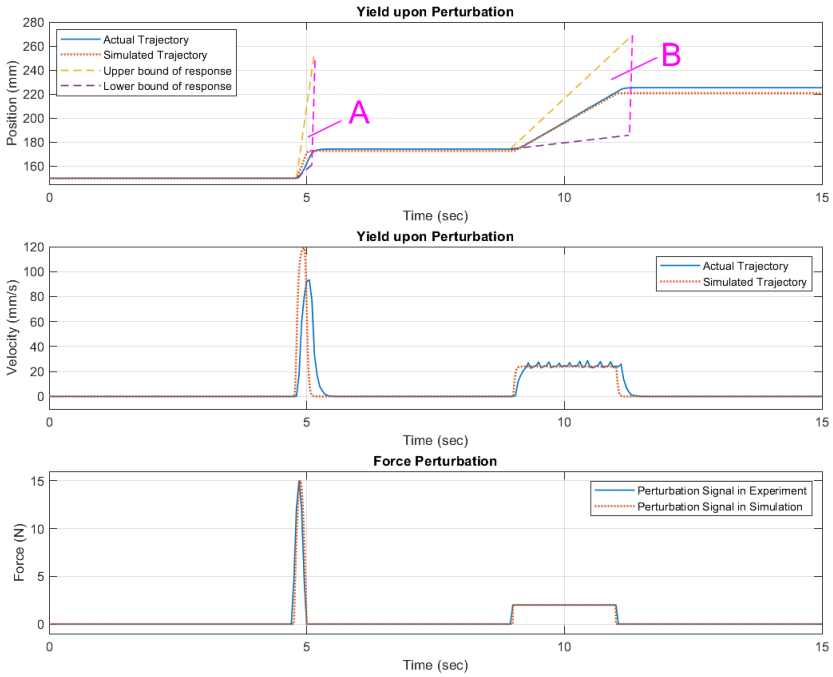

Figure 2.16. Test result for passive.

Performance for the experiment of switching from "trajectory tracking mode" to "force tracking mode" is shown in Fig. 2.17 first column. Tests start with a linear trajectory (3 DOF trajectory for experiment and 1 DOF for simulation). Switching signal is triggered upon reaching the drilling position, presumably planned via diagnosis. Performance for the experiment of switching from "trajectory tracking mode" to "passive mode" is shown in Fig. 2.17 first column. During tracking a linear trajectory (3 DOF trajectory for experiment and 1 DOF for simulation), the system switches into the passive state at t=8s during trajectory tracking to simulate an emergency pause. In force perturbed tests, a step force perturbation of 2N is generated around t=8s as well to test robustness. Performance for the experiment of switching from "force tracking mode" to "trajectory tracking mode" is shown in Fig. 2.17 second column where system switched at t=8s during force drilling into tracking a one DOF linear trajectory rising from 50mm, in order to simulate a decision to pause drilling

and retreat from the mouth following a certain trajectory. Performance for the experiment of switching from "force tracking mode" to "passive mode" is shown in Fig. 2.17 second column where system switched at t=8s during force drilling to passive state, in order to simulate an emergency pause during drilling process. Performance for the experiment of switching from "passive mode" to "trajectory tracking mode" is shown in Fig. 2.17 third column. System switched at t=8s during passive state into tracking a linear trajectory, in order to simulate the recovery from an emergency pause to trajectory tracking. In force perturbed tests, a step force perturbation of 2N is generated around t=8s. Performance for the experiment of switching from "passive mode" to "force tracking mode" is shown in Fig. 2.17 third column where system switched at t=8s in order to simulate a potential recovery from emergency pause into drilling process.

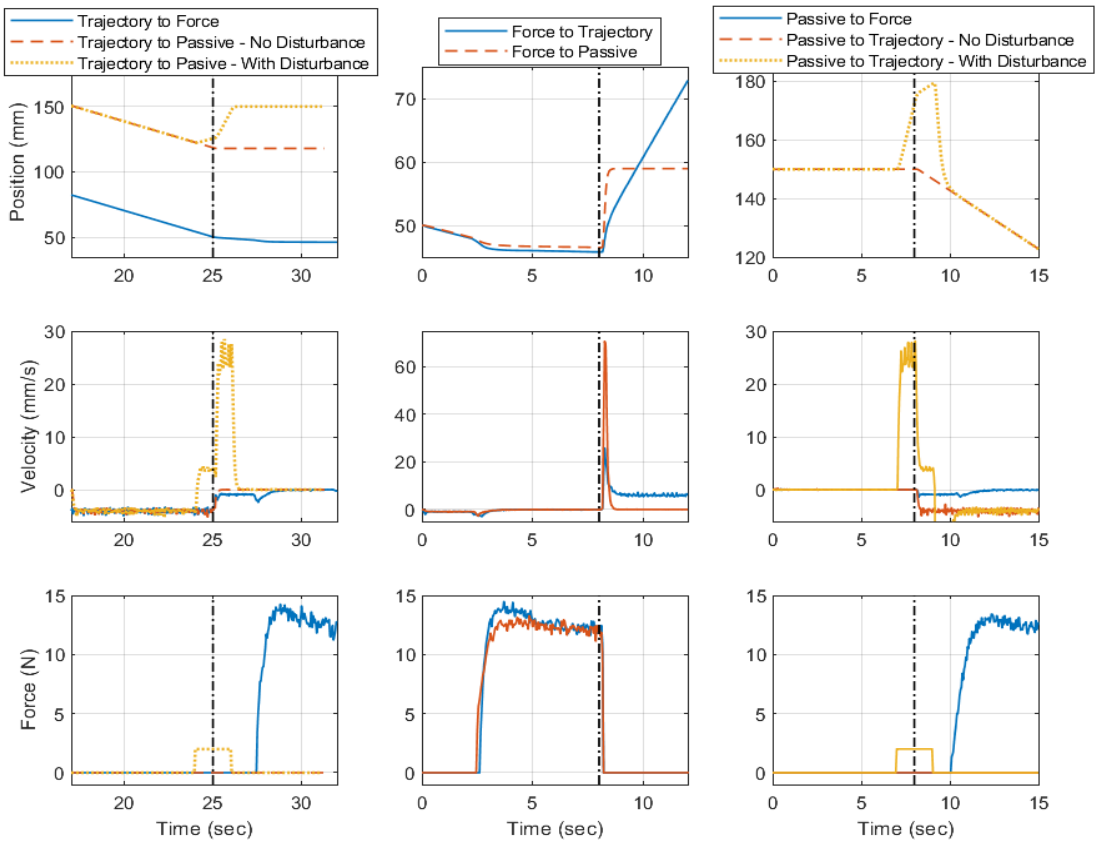

Figure 2.17. Test result for switching.

2.3.4. System demonstration

A demonstration of system integrating all functions is built to verify the design of the structure. Patient status identification is processed based on position measurement of the jaw model with MX digitizer. Denso arm starts from a home position and follows the decision of the robot to process the surgery. Fig. 11 shows some of the behaviors of the robot system. In (a) the "Approaching" process is disturbed by a contact force pushing up, robot trajectory then yields to the disturbance for instant protection. In (b) a slight motion is applied to the jaw by hand when the robot is in "Engage" state approaching the drilling target position. System takes an instant reaction in an attempt to retreat to

the safety position {S}. In (c) a large jaw motion is applied such that the system switches to passive state, and therefore will follow the motion of contact direction, In (d) the robot finds the drilling target position and proceeds with the drilling operation when the jaw only has negligible motion disturbance.

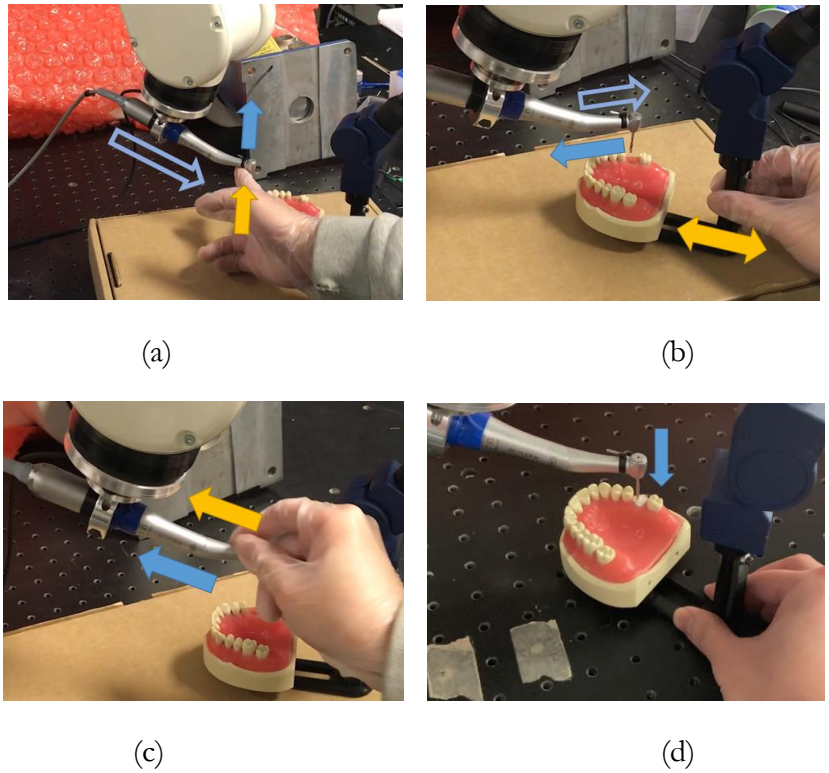

(a) (b)

(c) (d)

Figure 2.18. System demonstration: (a) Disturbing "Approach" stage, (b) Disturbing "Engage" stage, (c) Protection during "Passive" stage, (d) drilling operation.

2.4. Conclusion

In this chapter, a robotic surgery system that integrates the interaction between patient and manipulator during dental implant drilling tasks is proposed. The interaction is achieved via three major parts. The motion of the patient is measured and classified into different statuses that affects the surgery progress, and the status together with a signal of interruption that can be triggered by the

patient is fed through an FSM model for the proper response in logic signal. This logic signal is then executed by the SMASC control algorithm with a real-time switching of position/force tracking control goal.

The attention of interaction between patient and robot has inevitably escalated the complexity of the design. The activities of the patient could impact the surgery such that the system must be tuned to respond to the patient properly in a similar fashion of the human surgeon. Therefore, the system adopts the logic of a human surgeon as a guideline for handling pHRI during the surgery. The simulation result indicates that the logic of the system can indeed mimic a similar behavior as a human surgeon and in any case without an emergency the system will converge to a complete surgery task. As a consequence of introducing logic of the patient protection, the manipulator is required of capability of real-time switching between tracking target position and tracking desired contact force. Since a conventional PID control law has difficulty coping with such a task in a short but smooth transient period, we propose a SMASC law by taking advantage of both admittance dynamics and the continuous convergence of the sliding surface. Both simulation and experiments confirm that, with proper gains in a specific implant drilling surgical environment, the control law can transit among trajectory tracking, force tracking and passive protection behavior smoothly and almost instantly. This result enables the preliminary prototype test in a non-surgical environment where response of the patient is simulated by disturbing the jaw model position during a complete process of drilling. The test result indicates a proper response from the robot system. Our future work, therefore, will be to create a further simulated clinical implant drilling environment to evaluate the performance compared to the human surgeon. In the meanwhile, effort will be continued in upgrading the AI system for robustness interaction with potential machine learning algorithms.

Chapter 3

Tooth preparation for crowning

3.1. Methodology

The goal of this research is to design and test the capability of robotic milling in tooth preparation. The structure of the robot system is shown in fig 3.1. The robotic system consists of three major tasks: tooth scan, trajectory generation and tooth milling. Tooth scan task will use tools such as CBCT to generate the 3D model of target tooth in high precision. The surgeon then can plan the surgery and use the robot system to generate the milling path of crown preparation. Robot system will perform the surgical operation according to the trajectory. While all three tasks remain to be improved in commercial applications, the main effort on this paper is to generate a proper trajectory for a mandibular molar. The remaining discussion will be based on the assumption that a sufficiently accurate scanning of the target tooth can be obtained.

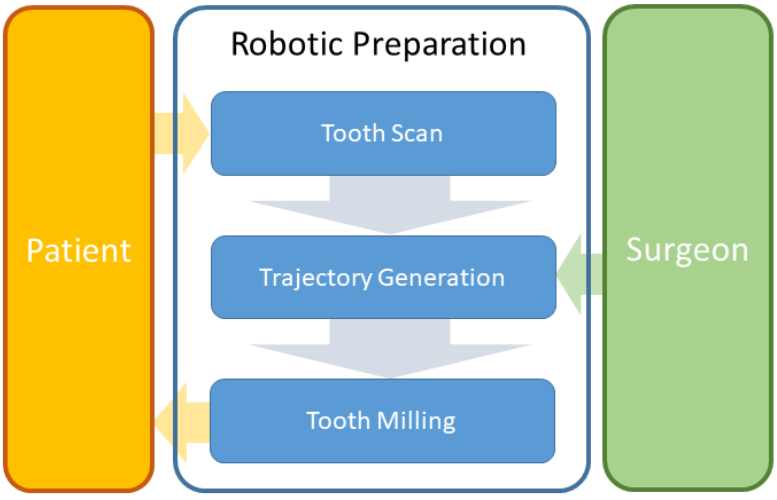

Figure 3.1. Robot system structure.

The process of crown preparation can be regarded as generating an axial wall and reducing the occlusal surface. The design of preparation involves multiple biologic, mechanical and esthetic considerations. The biologic concern requires the axial cut to take advantage of proximal enamel to avoid damaging adjacent teeth. The cut should avoid soft issues as well, which can be achieved by proper traction. Proper chemicals and cooling methods should be applied to protect the pulp. The design should conserve as much tooth structure as possible. A complete coverage is assumed with requirement of supragingival margin. The mechanical consideration requires retention and resistance against dislodging force via tooth preparation geometry, surface roughness, and adequate preparation margin. The esthetic considerations involve materials of the crown, which is assumed to be all-ceramic in this study.

The fundamental procedure of preparation is to create an axial wall and a proper occlusal surface for the crown. Therefore, it is natural to split the task of trajectory generation into generating an axial reduction trajectory, and an occlusal reduction trajectory. The axial reduction process creates a bounding surface that has a great impact on the crown's resistance to dislodging force. The taper angle of the surface is essential in the way that a taper angle too large will reduce the crown's resistance upon side contact force, while a taper angle too small can cause concentrated stress upon installation due to deformation. Depth of the wall, on the other hand, is another factor that will impact the quality of the crown. Therefore, a minimum depth of the axial wall should be ensured. Thickness of the reduction is important as well since we need to take advantage of the proximal enamel to avoid damaging adjacent teeth while avoid too much removal of the margin. Other concerns including preservation of the contours and profile of the original tooth, and proper design of a supragingival margin with proper geometry, should be taken into consideration as well. The robot system will remove the axial wall by the side of the bur, therefore a careful design of target tip position and orientation about the central

axis is crucial to fulfill the above design requirements. A proper milling speed is also important in efficiency of the surgery as well as to avoid overheating the pulp.

Removing the occlusal surface involves a requirement of effort to preserve the original geometry as well as an adequate reduction to prevent material deformation while maintaining sufficient depth of the axial wall. We propose two methods as solutions: V-shape cut and topographic cut. V-shape cut is to obtain a proper axis according to the geometry of the tooth to generate a V-shape valley that approximates the original occlusal surface. Robot will use the side of the bur to reduce the occlusal surface and remove sharp edges between axial wall and V-shape cut. In topographic cut, the robot will try to reduce a layer milling by tool tip following the original surface of the tooth. Sharp edges can be milled as well to blend the two surfaces.

3.2. Trajectory design

3.2.1. Axial reduction

As one basic requirement for both axial and occlusal reduction is to preserve the original shape or contour of the tooth, finding a proper reference axis is essential. Therefore, we take the supragingival part from the tooth scan as the operational part. To ensure a tall axial wall, the slicing surface is designed to be close to the gum as the outer contour of the bur tip surface as well. The principal axis and center of mass are calculated. The three principal axes are regarded as distal to mesial direction, lingual to buccal direction and the center axis. The center of mass is the coordinate origin. A sufficiently accurate registration of this coordinate with respect to the robot base frame is assumed. Fig 3.2 shows the coordinate system generated by Solidworks from a tooth scan. Target position of bur is then offset from the contour of the tooth slicing surface, assuming a round shape of bur tip with 1.1 mm diameter will create a smooth and even margin of axial wall with 1.2 mm thickness (fig.

3.3). The approaching angle can be found with a ZYZ Euler angle rotation. Consider the principal axis ${}^{Base}_{Principal}R = [I_x \quad I_y \quad I_z]$ defined with respect to the base frame, and a desired taper angle of the axial wall θ tilted towards the z axis from all positions along the trajectory. Then the approaching angle of tool tip orientation can be calculated by ${}^{Principal}_{Tip}R = R_z(\phi)R_Y(-\theta + \theta_{bur})R_z(\psi)$, where θ_{bur} is the bur's taper angle, ϕ is the projected angle between I_y and vector pointing from center of mass to target position on I_x-I_y plane, and ψ is the bur's axial angle. Note that a complete coverage of axial wall reduction will have ϕ span in $360^{\mathbf{o}}$ about I_z, and ψ must be chosen such that the hand piece can approach the position without collision in the oral space. In this study, $\theta_{bur} = 1.4°$, which can be considered acceptable as axial wall taper angle. Therefore, in order to minimize the robot motion range, we minimize the range of orientations by setting $\theta = 1.4°$ so that the bur can approach from an orientation that is vertically aligned to z axis direction, and $\psi = -\phi$ so that the handpiece can have a minimal orientation change during the task to reduce risk of collision with adjacent tooth, lips or other tissues.

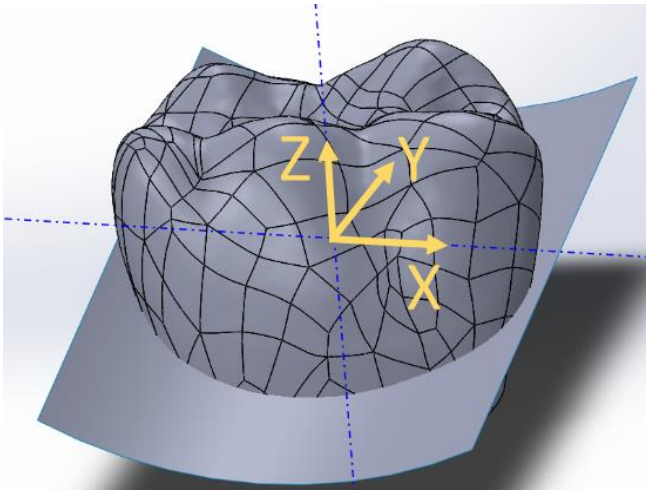

Figure 3.2. Principal coordinate of trajectory.

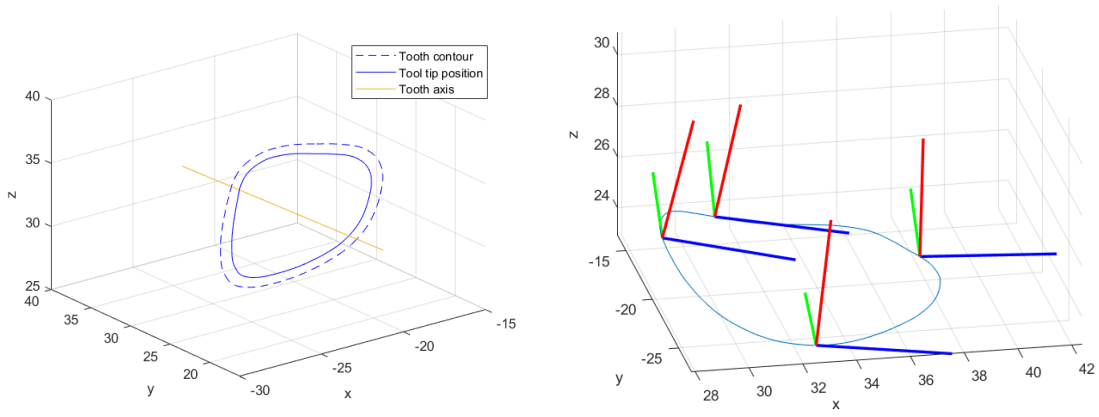

(a) (b)

Figure 3.3. Axial path design: (a) conserving contour, (b) axial trajectory path

3.2.2. V-shape occlusal reduction

The trajectory of V-shape is designed as a 4-step process: buccal side, lingual side, buccal chamfer, and lingual chamfer. To have a perfect chamfer that covers an even margin through all sharp edges the hand piece has to approach the target position from a large range of orientations, this would cause both higher risk of collision inside the oral space and higher difficulty in the design of the robot system. Therefore, a compromise has to be made to minimize the robot motion inside the mouth, instead of pursuing a perfect chamfer. We set the approach of buccal chamfer to be the same as cutting the lingual side, and lingual chamfer same as cutting buccal side. Fig. 3.4 shows the V-shape cutting process. The spline of valley is designed based on the principal coordinate I_x and geometric shape of the bur tip, and is bent at both ends to create part of the chamfer. The side surface has a 60-degree angle to I_z and a maximum axial wall depth of about 3 mm on both buccal and lingual sides. The path

of chamfer on both sides are designed following the contour of the sharp edges generated by axial reduction and the 60-degree side surface cut, the shape of round end bur is considered as well such that a chamfer of up to 1mm can be created along the sharp edges.

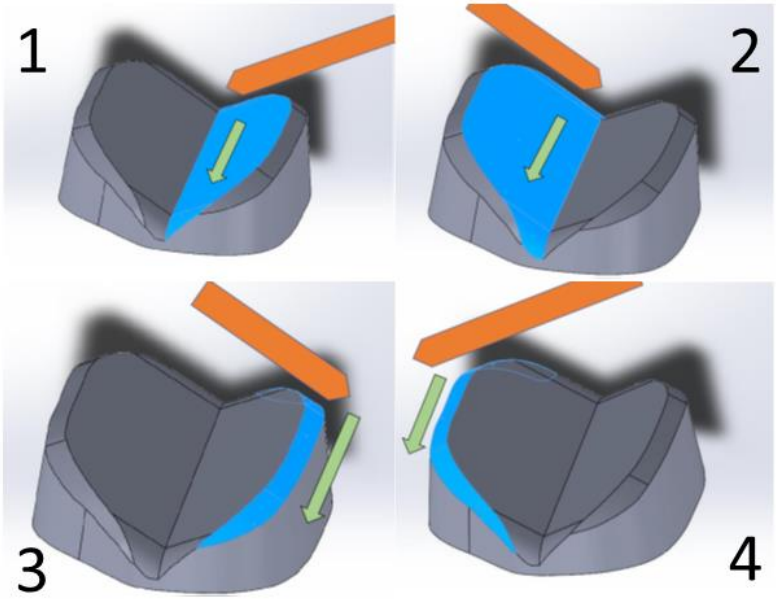

Figure 3.4. V-shape occlusal reduction.

3.2.3. Topographic occlusal reduction

The trajectory of topographic cut requires a high resolution of occlusal surface modeling (fig. 3.5). Since the occlusal surface will be reduced after the axial reduction, we do not have to mill the part that has already been removed by axial reduction. The actual target milling area can be obtained by CAD software by simulating the axial wall reduction (fig. 3.5(d)). The surface data is then converted to a mesh grid data for generating a tool path. Unlike in the V-shape method, the chamfer can be designed together with the target occlusal surface and milled by the tip of bur. To create the chamfer without

removing the original contour of the tooth, we shift the mesh grid data by reducing the edge of contour. Fig. 3.5(e) shows the concept of chamfer generation process. In this study we set an edge chamfer of 1mm within 1 mm region to the edge. One significant advantage of this method is that it can help reproduce the original surface and thus fulfill the requirements from biologic and mechanical consideration in preparation design. However, since the limited oral space will constrain the bur's approaching angle, the tool tip cannot be assumed to be able to reach the surface from a vertical direction. This yields to the problem that a tilted orientation of bur could remove some features of the occlusal surface. The maximum descending and ascending gradient of the surface is 79.1 degree along X direction (Buccal - Lingual), and 72.8 degree along Y direction (Mesial - Distal). The trajectory is planned to follow a Y direction back and forth S shape path to cover entire milling surface, and the bur has a 1.4 degree taper angle which means the maximum tolerance for gradient magnitude is approximately 88.6 degree, the trajectory design will not remove surface features along Y direction as long as the bur insertion angle can be aligned with the I_x-I_z plane. However, a safe approaching angle of 60 degrees is assumed along X direction in order to avoid collision in the oral space as stated above. To enforce this constraint, the target occlusal surface has to be modified. Mesh grid is adjusted to have the gradient along X direction being capped at a maximum of 60 degrees. If the surface gradient exceeds, adjacent mesh points height will be adjusted accordingly.

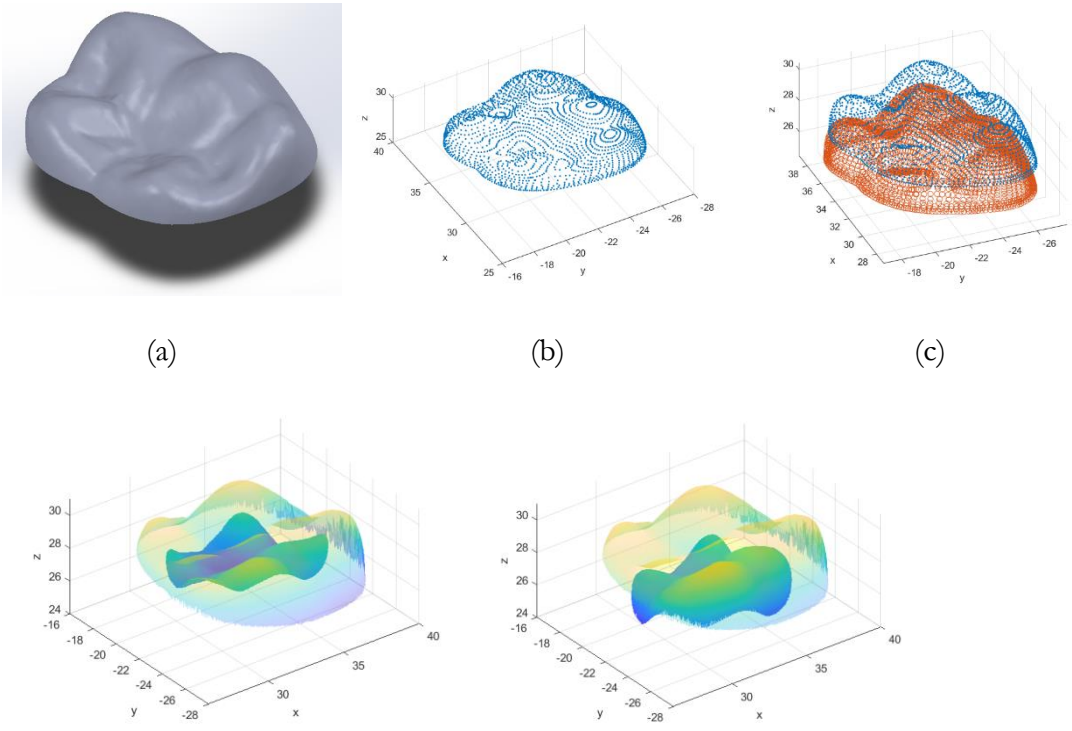

Figure 3.5. Occlusal trajectory design: (a) Occlusal surface; (b) sampling of the occlusal surface; (c) offsetting target occlusal surface; (d) effective region of occlusal reduction after axial reduction; (e) edge chamfer upon target occlusal surface.

Another problem is caused by the irregular shape of the target occlusal surface being milled by a round end bur shape. The robot can control the tooltip target position, which marks the center of the round end, to follow a straight path but the irregular surface yields to an irregular path of the actual

milling contact trajectory. Therefore, to make sure the actual milling contact will cover the entire surface by moving back and forth along Y direction as a straight line as possible, the trajectory of the tooltip must be adjusted according to the normal direction of the surface at desired contact position. The tool tip position is calculated by offsetting along the surface normal direction by the tip's radius, and a low pass filter is applied to improve the smoothness of the path. Fig. 3.6 shows the result of the design of topographic occlusal cut trajectory. Note that the surface modification by capping the maximum gradient is based on the assumption that the surface shape will not be altered too far from the original shape. This is often related to how many mesh grid points lie beyond the maximum gradient and how much they exceed the maximum. If for some reason the original surface shape goes too far from the maximum gradient, such as a cavity, this method might fail and other methods must be considered. In this study, we assume an ordinary molar without cavity or other uncommon occlusal surface, that the maximum gradient method will conserve most of the original occlusal surface features. It is also worth mentioning that the robot's path control can have a major influence in the performance of such high precision milling task. One can command the robot to reach the exact target positions designed following the above method, however, in order to ensure the position accuracy, the robot motion control will have to decelerate upon closing to the target position till target position has been reached. This means the robot motion control will be running at a frequent deceleration or low average speed through the milling trajectory and will dramatically consume more time to finish the task. One way to increase the efficiency is to allow the robot motion control to move past the current via point to the next one when the end effector is within a certain "blending" region. This region can be seen as an extra error tolerance that will reduce the deceleration, and therefore increase motion speed, at the cost of increased tracking error. In the later experiment, we will set the robot to

have different blending settings to verify the relation between surface milling quality and the completion time of the task.

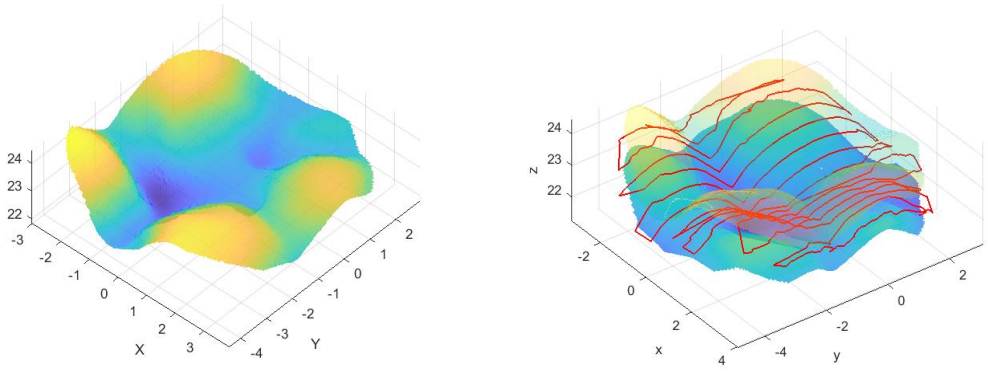

(a) (b)

Figure 3.6. Path design of occlusal reduction surface: (a) original occlusal surface to be reduced; (b) target occlusal surface with adjustment on gradient and cutting path (red line)

3.3. Experimental protocol

3.3.1. Simulation software

A dental simulation software is programmed to check the trajectory inside the oral space for orientation and contact. Fig. 3.7 shows a dental handpiece following the trajectory, the red oval ring indicates the lips. The semi-transparent shape is the target tooth outline and the dark gray region indicates a rough design of the tooth in V-shape. Simulation software supports different types of hand piece and different shape of the bur; to verify the path we chose a straight shape of hand piece with a cylinder bur. Once the orientation and position of the milling path meets the design purpose, we move on to the robotic milling test for actual cuts.

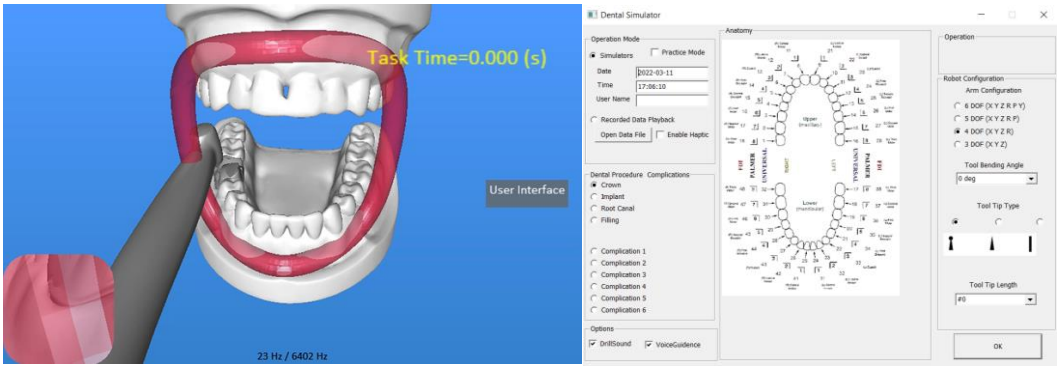

(a) (b)

Figure 3.7. Dental simulator: (a) simulation process; (b) user interface

3.3.2. Equipment Setup

The experiment device is built based on a Mecademic Meca 500 robot (fig. 3.8). An air turbine driven handpiece controlled by NSK Ti-Max NL400 unit is mounted to the robot wrist via an ATI mini 40 force/torque sensor. A 3D printed tooth model from a tooth scan is mounted on the calibration block that is fixed to the same platform as Meca robot. The target base position of the printed tooth model is measured by a Microscribe MX digitizer. The registration of the target tooth is done by converting the principal axis and mass center coordinate designed via Solidworks into the measurement printed tooth model base with respect to the robot's base. The force sensor is used in calibration and registration of the tool frame to the robot's wrist frame, which is to detect bur tip contact on the calibration block. The trajectory is controlled by Microsoft Visual Studio C++ from the PC. The control signal is sent to Meca robot via TCP connection, designating target position, maximum motion speed and blending (interpolation passing through via points) setting. The

trajectories of axial reduction and occlusal reduction are combined into a single task that a complete cut of the preparation will be performed. The cutting result with different settings will be examined.

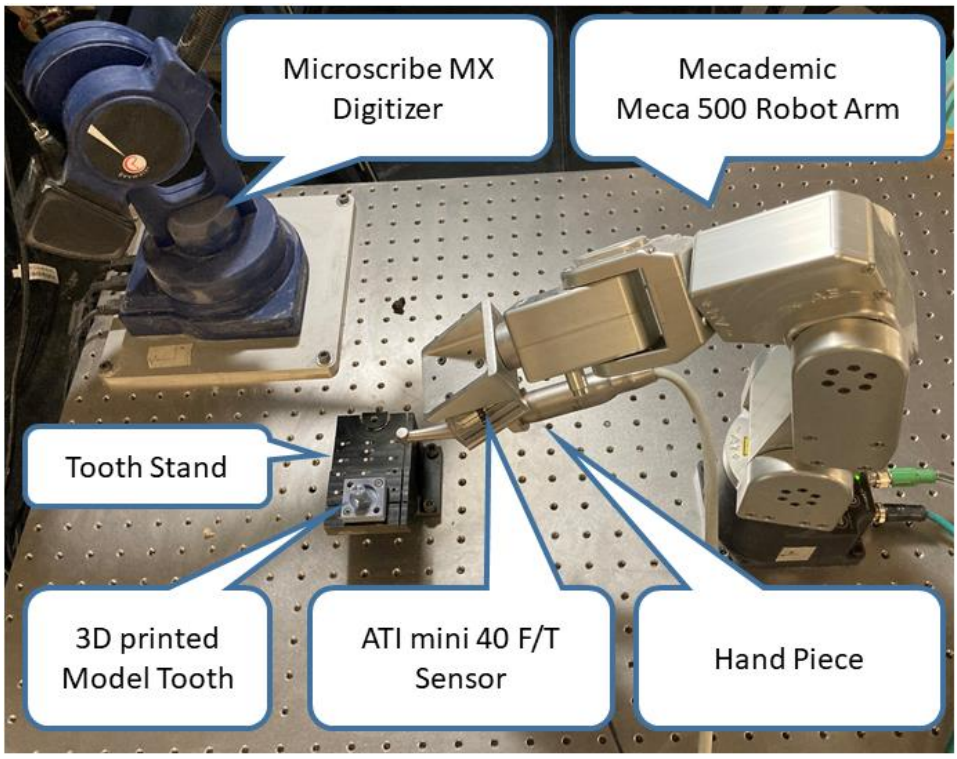

Figure 3.8. Equipment setup.

3.4. Result and discussion

Fig. 3.9 shows the cutting process of the V-shape with axial reduction. The handpiece approaches from home position to the tooth and cuts the axial wall following the original contour of the tooth and generates an even margin of 1 mm with a small and smooth taper angle towards the center of the tooth. Hand piece then returns to home position and approaches again to cut the two sides of the V-shape. It then approaches the sharp edges and creates the chamfer on both sides with the same orientation as in cutting the sides.

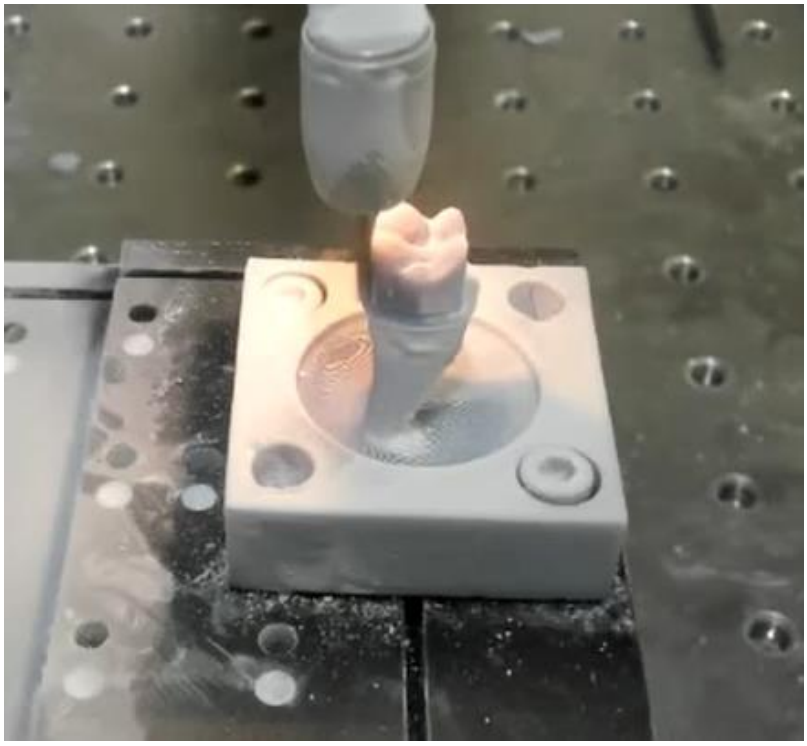

(a) Axial reduction

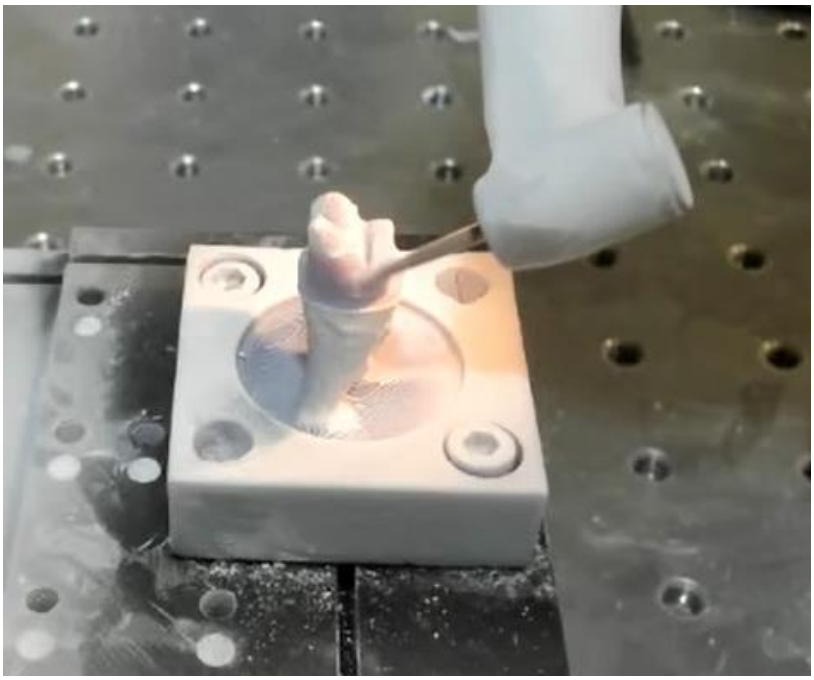

(b) V-shape occlusal reduction on buccal side

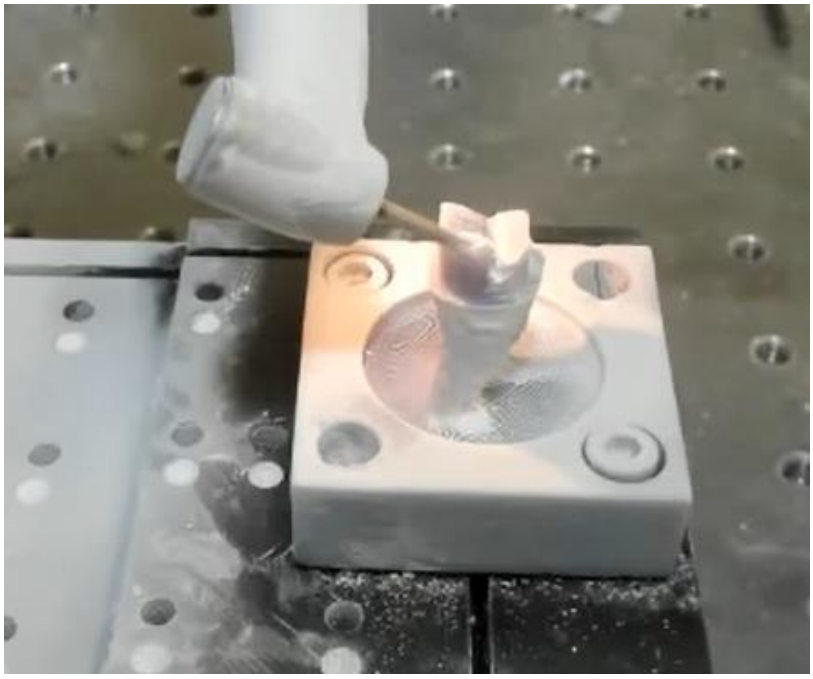

(c) V-shape occlusal reduction on lingual side

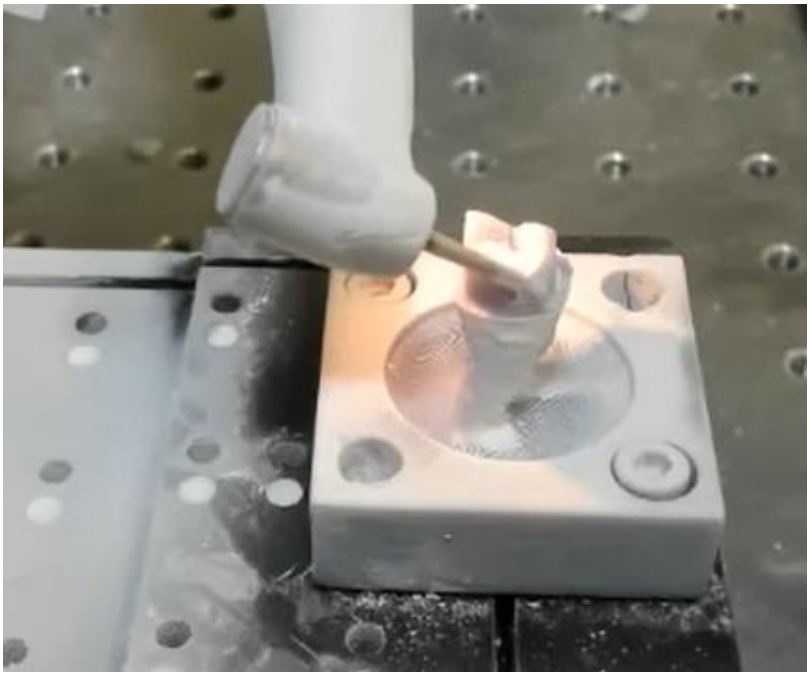

(d) V-shape occlusal chamfer on buccal side

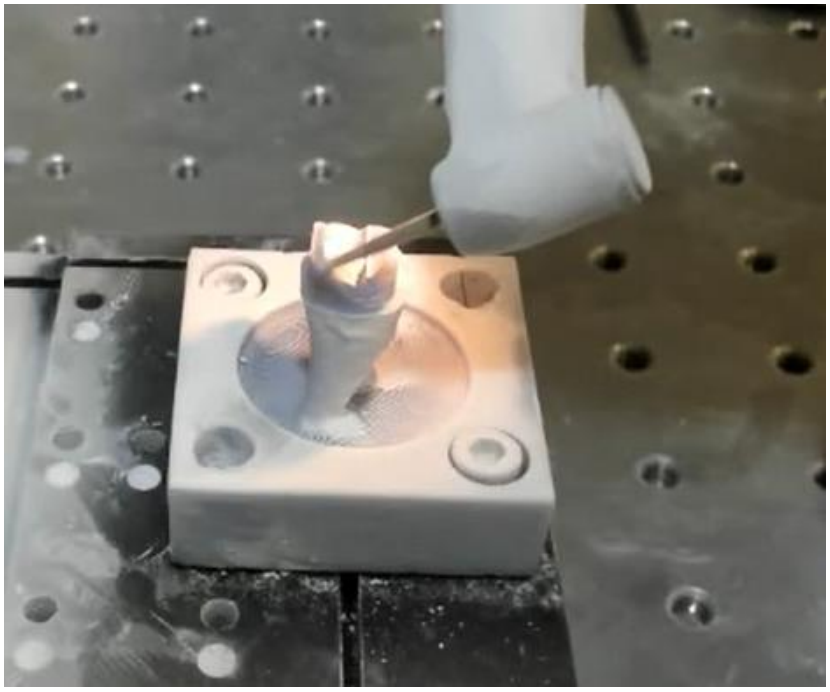

(e) V-shape occlusal chamfer on lingual side

Figure 3.9. Axial reduction and V-shape Occlusal reduction.

The hand piece approaches from the home position to the tooth for an axial reduction cut. Once the axial wall is generated the hand piece returns to the home position and commences the topographic cut. Fig. 3.10 shows the cutting process of the topographic cut.

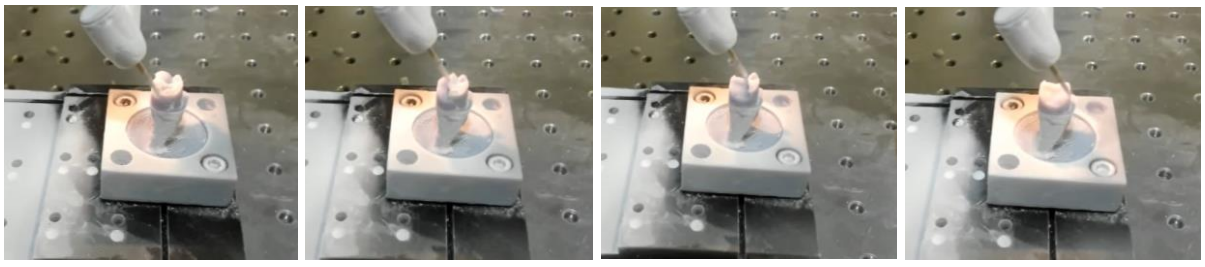

Figure 3.10. Topographic occlusal reduction (in time sequence from left to right).

Fig. 3.11 shows the comparison of different cutting results in speed and accurate setting for topographic occlusal cut. High accuracy settings result in a smooth occlusal surface at the cost of surgical time.

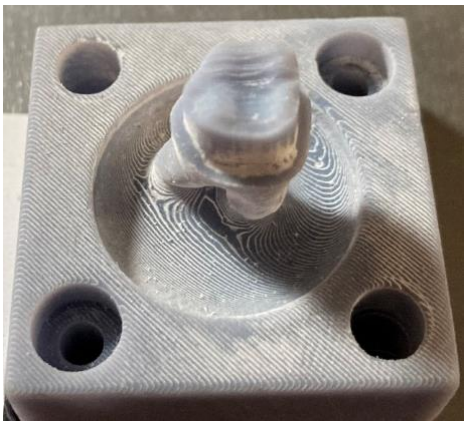

(a) 100% blending, task time: 16 secs

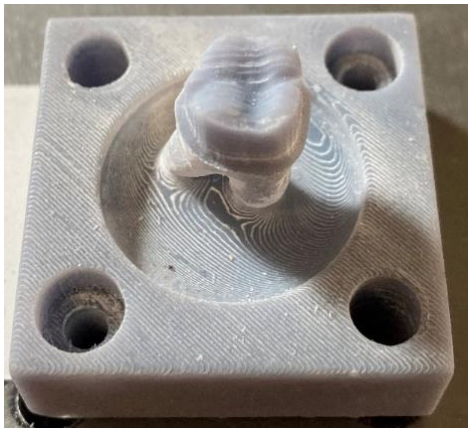

(b) 90% blending, task time: 50 secs

(c) 0% blending, task time: 300 secs

Figure 3.11. Occlusal cutting results in different settings.

3.5. Conclusion

In this study, the robotic tooth preparation process is investigated and the trajectory is generated and tested. The tooth preparation process can be improved by robot with improved accuracy and efficiency, however, the irregular shape of the tooth and limited oral space for the task present a great challenge to the design of the robot system. The design of axial reduction and occlusal reduction path involves considerations in biology, mechanics, and aesthetics thus the trajectory design must fulfill the requirements in reducing a proper thickness in the coverage of the tooth, conserving original tooth contour, avoiding collision in oral space, and minimizing the robot motion range. In order to achieve the requirements, the trajectory is designed based on a scan of the tooth with a supragingival slicing that separates the operational part of the tooth. Principal axis of this operational part is found and the axial wall with taper angle will conserve the contour of the tooth shape with an even margin design taking advantage of the bur's round end shape. For occlusal trajectory we proposed two methods with

different focuses on either efficiency or quality. The V-shape cutting method creates straight valleys with limited chamfers to remove sharp edges, and the topographic cut conserves the original surface but is more complicated and may require further extension in the algorithms to cope with specific type of the tooth. Both simulations and tests verifies the effectiveness of the trajectory design. The cutting experiment of axial reduction indicates a smooth and even margin with proper taper angle for the installation of crown. The cutting experiment of V-shape occlusal reduction proves that the tooth can be prepared as in the designed shape. The topographic occlusal reduction further shows the relation between robot accuracy and the time efficiency for this method. The future work will be focused on quantitative analysis on the tooth cut, and design of a full trajectory for the surgery process.

Chapter 4

Simulation of teleoperation control in eye surgery

4.1. Methodology

4.1.1. Control method

The structure of tele-operated control robot system (fig.) takes input command from master arm and convert into slave arm motion command. A commonly used strategy in robotics is to take input via Cartesian coordinates in operational space and map it into slave arm target position in relative motion. In eye surgery, the fact that the tool penetrates into the eyeball through the pivot position makes it a 4 degree of freedom task as the planar motion tangent to the eyeball sphere on pivot position is constrained. Therefore, the mapping from master arm to slave arm becomes $dx_{master} = \{dp_x^{master}, dp_y^{master}, dp_z^{master}, d\theta^{master}\}$ into $dx_{slave} = \{dp_x^{slave}, dp_y^{slave}, dp_z^{slave}, d\theta^{slave}\}$, where θ^{master} and θ^{master} are rolling along the tool axis. This method allows the operator to control the position of the slave arm tool tip by moving the master arm towards the same direction, as if the operator is holding the tool tip position inside the eye ball. We call this control method as "inside control". However, conventional eye surgery requires the surgeon to operate the instrument by holding not the tool tip but a position outside the eyeball, which we call "outside control". Such approach can be achieved by mapping the spherical coordinates in master arm operational space $dx_{master} = \{\mathrm{d}\Phi^{master}, \mathrm{d}\Psi^{master}, dR^{master}, d\theta^{master}\}$ into slave arm target position. Φ^{master}, Ψ^{master} and R^{master} denote the master arm end effector's pitch, yaw and insertion. Operator controls the tooltip position in this method as if holding the surgical instrument in a conventional eye surgery. Although inside control mode has been a default in many surgical robot system, the outside

control mode could be more intuitive to experienced eye surgeon and therefore further test is necessary to compare the performance between the two control methods.

4.1.2. Scaling factor

The mapping between master arm and slave arm can greatly affect the operator's performance. A scaling factor can be placed to help with the performance.

$$dx^{master}{}_{4\times1} = \alpha_{4\times1} \circ dx^{slave}{}_{4\times1}$$

Where $\alpha_{4\times1}$ is the scaling factor on each degree of freedom. Since rotation is involved, scaling on rotation could potentially create disorientation to the operator along time, therefore we set scaling on all direction with respect to rotation to be 1, including pitch Φ, yaw Ψ for outside control as well as rolling θ for both control methods. Similarly we set scaling on p_x, p_y and p_z to be the same value to avoid the potential disorientation issue. A small scaling factor indicates agile motion for slave arm but also makes it vulnerable to noise and disturbance. A large scaling factor, on the contrary, stabilizes the slave arm motion at the cost of increased master arm travelling distance. Therefore, finding a proper value or range of the scaling factor is also one of the goals of this research.

4.1.3. Virtual reality (VR) environment

In order to evaluate the performance as close to a clinical environment as possible. The tasks for experiments must be designed to cover common practices in an eye surgery, and a VR simulation environment is adopted for teleoperation tasks. The surgeon must perform basic operations such as reaching target positions, grasping targets, holding the tool at target position, or following specific paths. The VR environment provides a panoramic view that gives the operators a better interpretation of the tool space compared to traditional video images. There are many types of feedback a simulation

environment can provide including visual effect, sound and haptic feedback. The operations involve cautious motion in both rotation and translation, a sound feedback could distract the operator, and torque feedback on the direction of rotation could have unknown impact on the operator's interpretation of contact direction when holding the handle with a few fingers. Therefore, in this study we only adopt the visual feedback presented as a bleeding effect when the tool penetrates the retina surface. Fig. 4.1 shows the structure of the system.

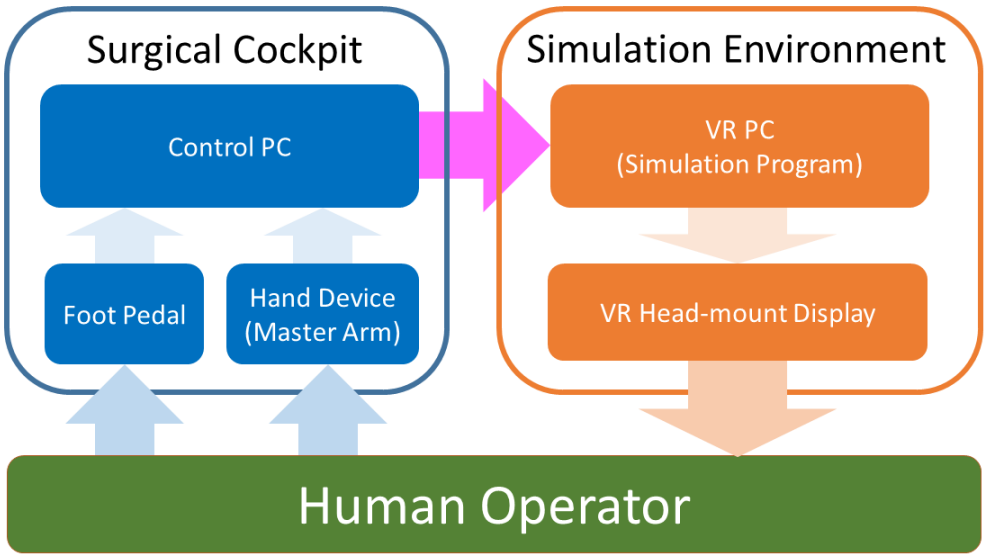

Figure 4.1. Simulation system.

4.2. Experimental protocol

4.2.1. Equipment

The cockpit device is constructed based on 2 master arms and a foot pedal. The master arm has 6 DOFs plus an extra open/close degree of freedom controlled by the gripper handle. Only the right

arm is used in this experiment. The foot pedal operates as a clutch that can start teleoperation or disengage. When starting with the foot pedal, slave arm in virtual environment will take velocity commands from master arm motion. When disengaging with the foot pedal during operations, slave arm will maintain current position. The intermediate control consists of a control PC and a VR PC, which are connected in a network. The control PC receives master arm motion data, controls master arm gravity compensation, and sends motion commands to the slave arm in virtual environment. Control algorithms are programed with Microsoft VC++ and Chai3D. The VR PC receives slave arm motion commands, generates a VR environment for display, and provides data measurements for analysis. The VR environment is programmed with Microsoft C#, Blender and Unity. The slave arm is displayed in VR environment with an Oculus Rift S head-mount display. The setup of the system is shown in Fig. 4.2

Figure 4.2. simulation equipment and surgical cockpit.

4.2.2. Task design

In order to cover various motions that could be involved during an eye surgery, four tasks are designed to examine the performance for different control settings in different surgical operations. The first task is "touch and reset" which is a basic training task to examine positioning tools to the target. The test subject controls a needle tip to touch each of the four target spheres in clockwise order starting with the bottom left one (Fig. 4.3). The target spheres have a diameter of 0.1mm and 5.5mm to the task space center, starting at 45 degrees every 90 degrees. The tooltip starts with a "reset area" of 0.2mm diameter in the center, and it must return to this area after each successful touch before moving on to the next sphere. Having the needle tip reach the target sphere or reset area and maintain position within the spherical area for one second is considered a successful touch. Task ends by the last successful touch with the reset area. To evaluate the performance, three metrics are examined: completion time, accumulated trajectory, and accumulated contact. Completion time records task time from the start within the reset area up to the final touch with the reset area. A good performance should be able to finish the task within a limited time period. Accumulated trajectory is the total traveling distance of the tool tip during the tasks. A small traveling distance for the task indicates a stable motion and low chance of collision damage. Accumulated contact integrates all penetration below the retina surface and indicates total damage done to the retina during the task.

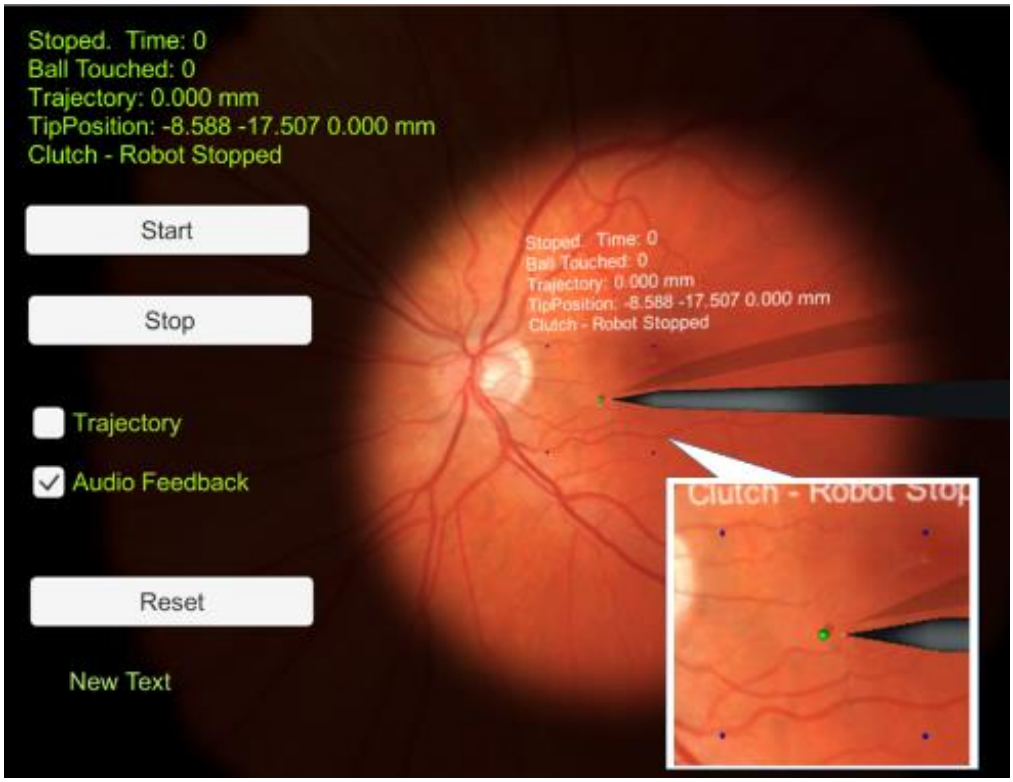

Figure 4.3. Task 1: touch and reset.

The second task is "grasp and drop" which is an advanced task based on the first one (Fig. 4.4). The test subject needs to control forceps to reach and grasp each of the four spheres and drop them to the reset area in the same order as in task 1. The geometry of the spheres is the same as in task 1. Maintaining contact for one second is considered a successful grasp or drop. Task starts and ends with the reset area. The same three metrics of completion time, accumulated trajectory and accumulated penetration are to be analyzed.

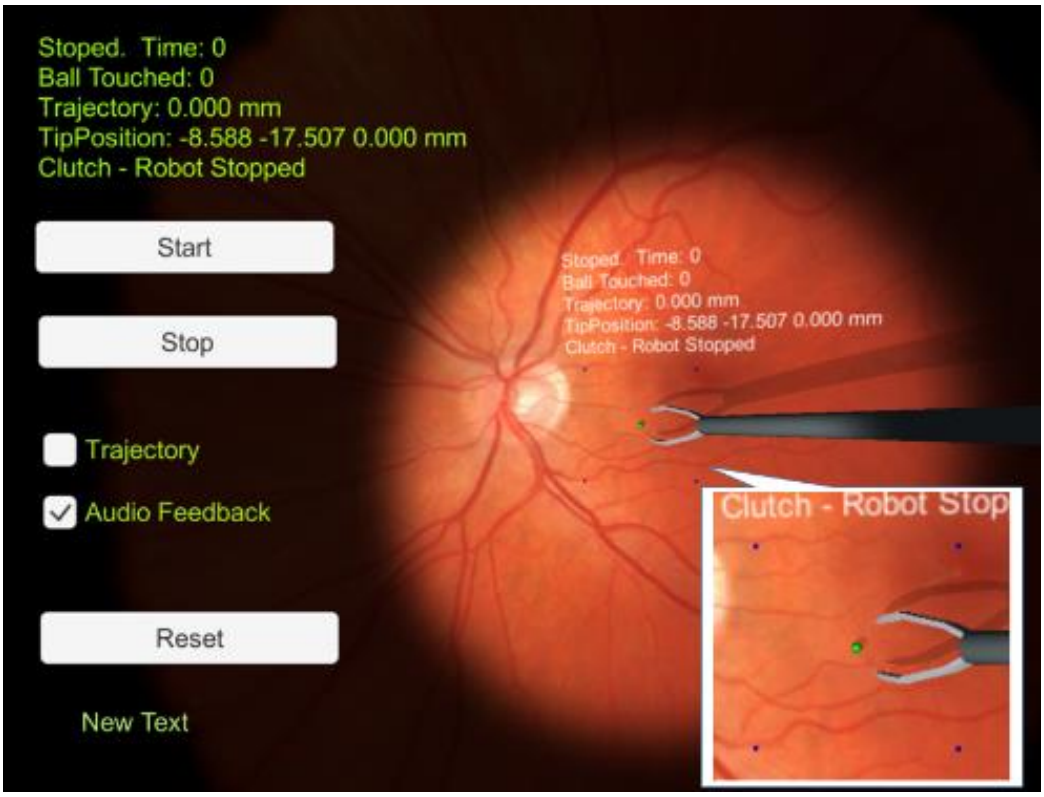

Figure 4.4. Task 2: grasp and drop.

The third task is "injection" which requires the test subject to locate the needle tip to a target sphere of 0.1mm diameter and maintain contact for 60 seconds (Fig. 4.5). Task triggers a timer upon reaching the target sphere and ends after 60 seconds. Four metrics will be examined for performance in this task: accumulated trajectory, accumulated penetration, average error, and accumulated trajectory out of target area. Accumulated trajectory measures the total tool tip traveling distance and accumulated penetration measures total damage to the retina. Average error evaluates an overall accuracy during injection. Accumulated motion out of the target area integrates traveling outside the 0.1 diameter error tolerance of the target sphere and could indicate a chance of failure by missing the target location during injection.

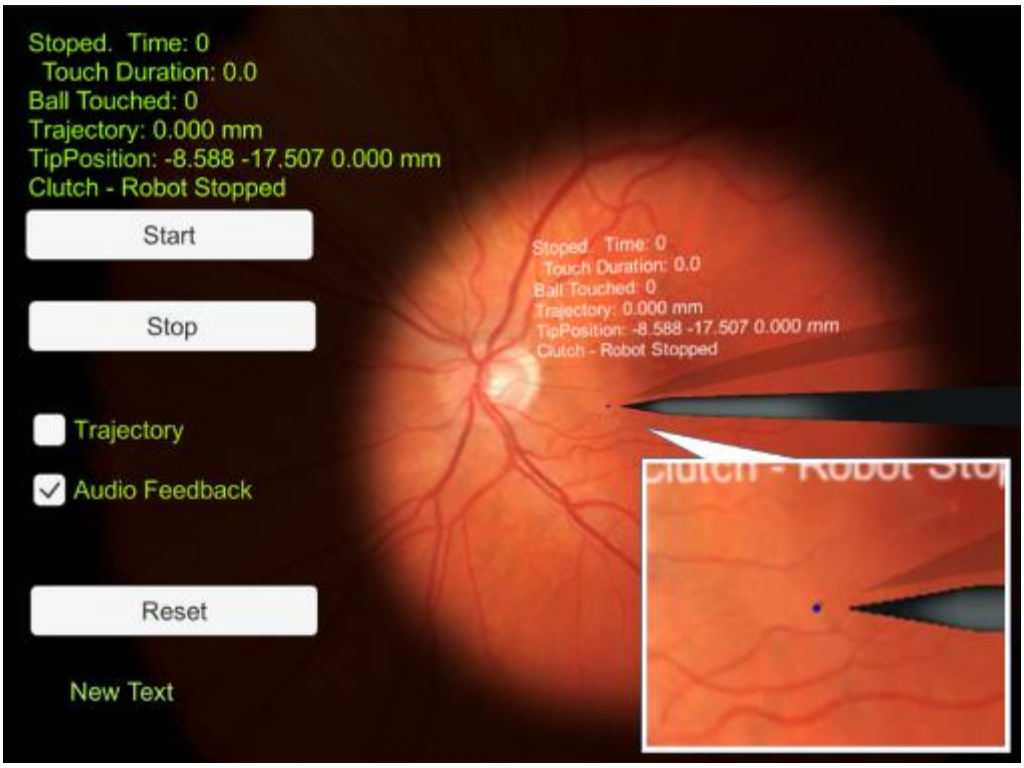

Figure 4.5. Task 3: injection.

The fourth task is "circular tracking" that requires the test subject to control the needle tool tip to drive a sphere of 0.1mm diameter to travel within a circular ring with 5.5mm diameter and 0.15mm radius of section area in clockwise direction (Fig. 4.6). The task is designed with relevant motions of peeling operations. It starts with the first reach of the target sphere and ends when the sphere finishes traveling for one lap. Five metrics are measured to evaluate the performance: completion time, accumulated trajectory, accumulated penetration, average error, accumulated trajectory out of tracking area. Completion time measures total time of the task. Accumulated trajectory measures total traveling distance. Accumulated penetration measures the total damage to the retina. Average error measures overall accuracy of tracking, and accumulated motion out of tracking area integrates the traveling outside the circular ring for chances of failure due to missing the target position.

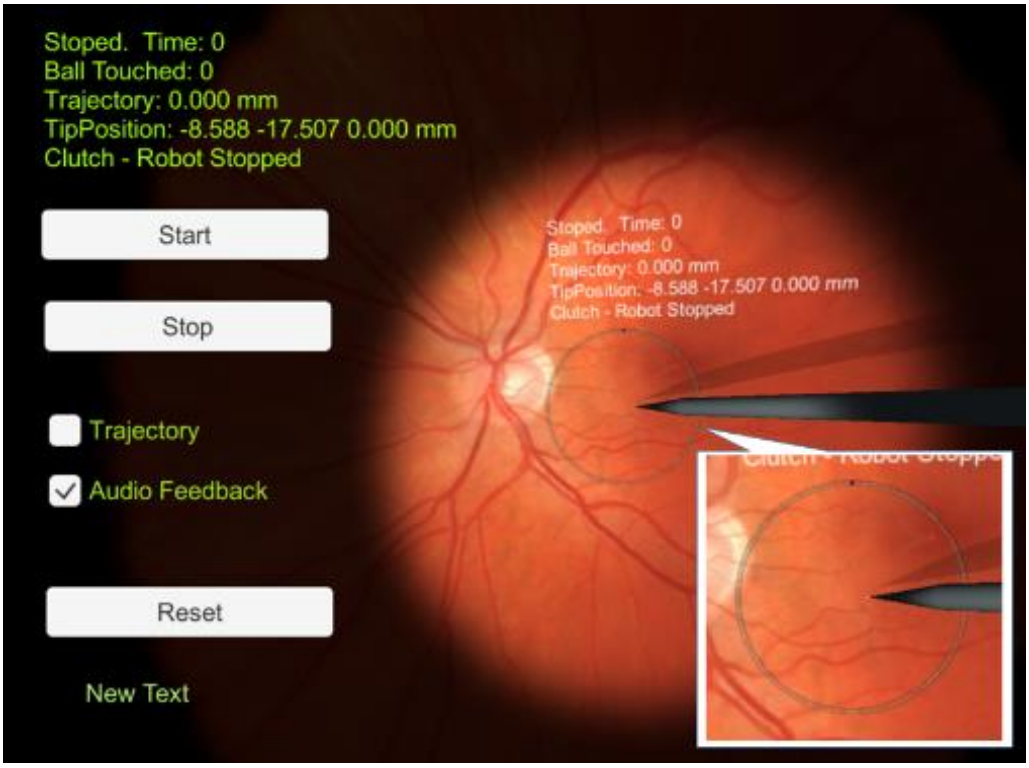

Figure 4.6. Task 4: circular tracking.

4.2.3. Experiment design

From preliminary tests, the master arm motion measurement in sub-millimeter level is subject to delay and noise from mechanical devices, especially for translation measurement. Such noise can further disturb the surgeon's operation when the scaling factor is low. However, as scaling factor increases, the disturbance on slave arm side will decrease since slave arm motion becomes less sensitive to motions of master arm. The preliminary tests suggest a minimum translation scaling factor of 5 in order to reject disturbance. Due to a direct measurement of pitch, yaw and roll joint motors from the master arm, the orientation measurement is less sensitive to disturbance and a scaling factor of 1 can be achieved for orientations in outside control mode. The upper bound of the scaling factor can be constrained by the range of the master arm. Preliminary test reveals a maximum scaling factor of 30 to complete tasks within range of the master arm. Therefore, we group the tests for inside control

mode into scaling factor 5, 10, 20, and 30. For outside control mode, scaling of pitch and yaw is fixed at 1 in order to avoid potential disorientation during operation, and scaling of insertion is fixed at 5 since preliminary test suggests a large difference of scaling between insertion and orientations could result in disorientation as well. In summary, 4 scaling factors for inside control and 1 for outside control will be tested for each of the 4 tasks.

One common issue that will affect the surgeons' performance besides control modes and scaling factors is the learning curve. To avoid insufficient training and overtraining through the tasks, all test subjects are given up to one-minute practice. During practice they can use the clutch or arm rest to adjust master arm to the most comfortable initial position individually. Clutch function is not allowed during the task. The order of tasks is randomized for each test subject so that the data does not indicates overtraining for certain tasks. Motion data is collected from 5 experts in eye surgeon, and 5 novices for comparison and validation. Metrics for each tasks are calculated based on collected motion data. Ten participants were enrolled in the study, including five ophthalmologists with vitreoretinal surgical training (experienced surgeons) and five engineers with no surgical experience (non-surgeons). All subjects were at least 18 years old, possessed normal sensory and motor function in their arms and hands, and had normal or corrected- to- normal visual acuity. All subjects were presented with a detailed information sheet on what the study entailed and all expressed verbal consent to participate. The study protocol received approval from the University of California Los Angeles Institutional Review Board (IRB#20-001861) and adhered to the tenets of the Declaration of Helsinki.

4.3. Result and discussion

The test result of completion time, accumulated trajectory and penetration in task 1 is shown in fig 4.7. For task time, inside control has a slight advantage over outside control, led by the best

performance of scaling factor 10 in expert group and a clearer advantage in non-expert group led by scaling factor 10. The accumulated trajectory indicates scaling factor 30 to be superior for both expert group and non-expert group. Both scaling factors 20 and 30 have good performance in avoiding damage to the retina. The test result of completion time, accumulated trajectory and penetration in task 2 is shown in fig. The performance among scaling factors in completion time and accumulated trajectory shows similar trends as in task 1. The best performance in completion time for experts is 20, 10 for non-expert, while 30 being best performance in accumulated trajectory for both groups. For accumulated penetration, best performance in both groups is scaling factor 20.

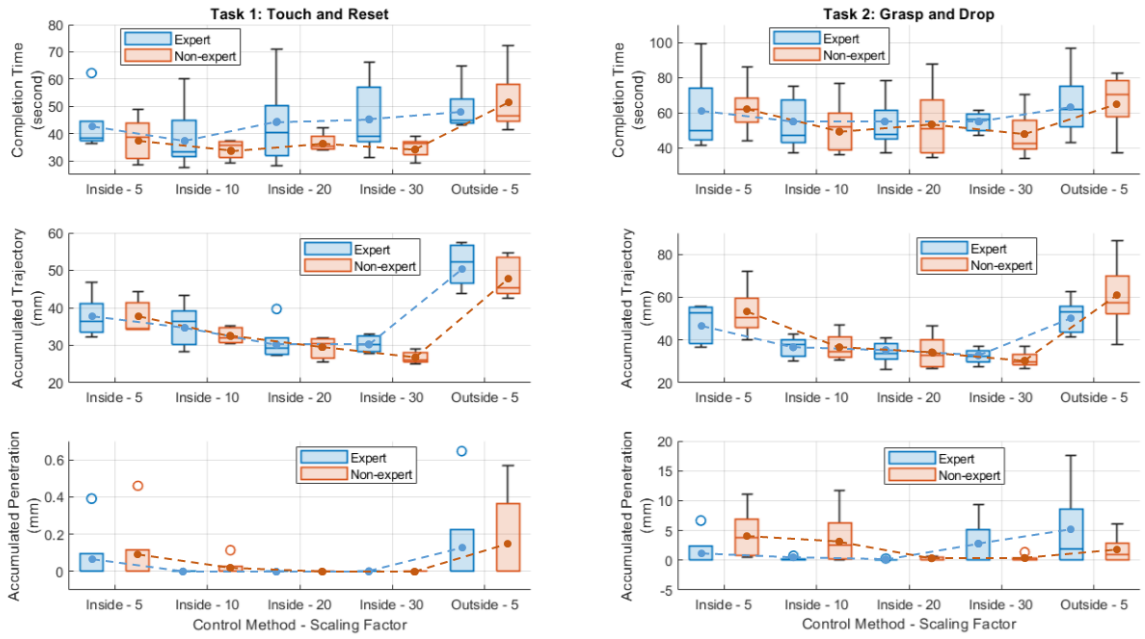

Figure 4.7. Performance for task 1 and task 2.

The test result of accumulated trajectory, accumulated penetration, average error, and accumulated trajectory out of target area in task 3 is shown in fig 4.8. The scaling factor 30 has the best performance in accumulated trajectory and accumulated trajectory out of the target in both expert and non-expert

groups. For accumulated penetration all scaling factors in the inside control mode successfully avoided damage on the retina. The performance of all scaling factors are close, with expert group 20 and non-expert group outside mode 5.

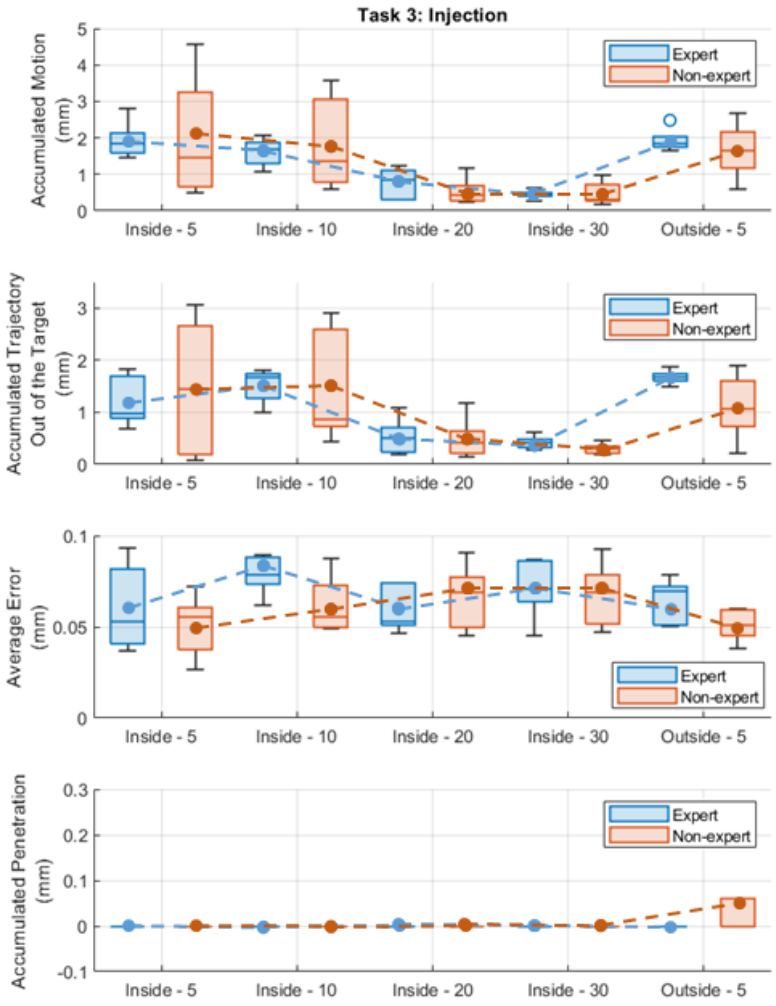

Figure 4.8. Performance for task 3.

The test result of completion time, accumulated trajectory, accumulated penetration, average error, accumulated trajectory out of the tracking area in task 4 is shown in fig 4.9. The scaling factor 30 of

inside control has the best performance in completion time of all metrics. For the non-expert group, inside 20 has the best performance in completion time, accumulated trajectory, and accumulated trajectory out of target. For accumulated penetration, the non-expert group has best performance at inside scaling factor 20, and inside 20 and 30 for average error.

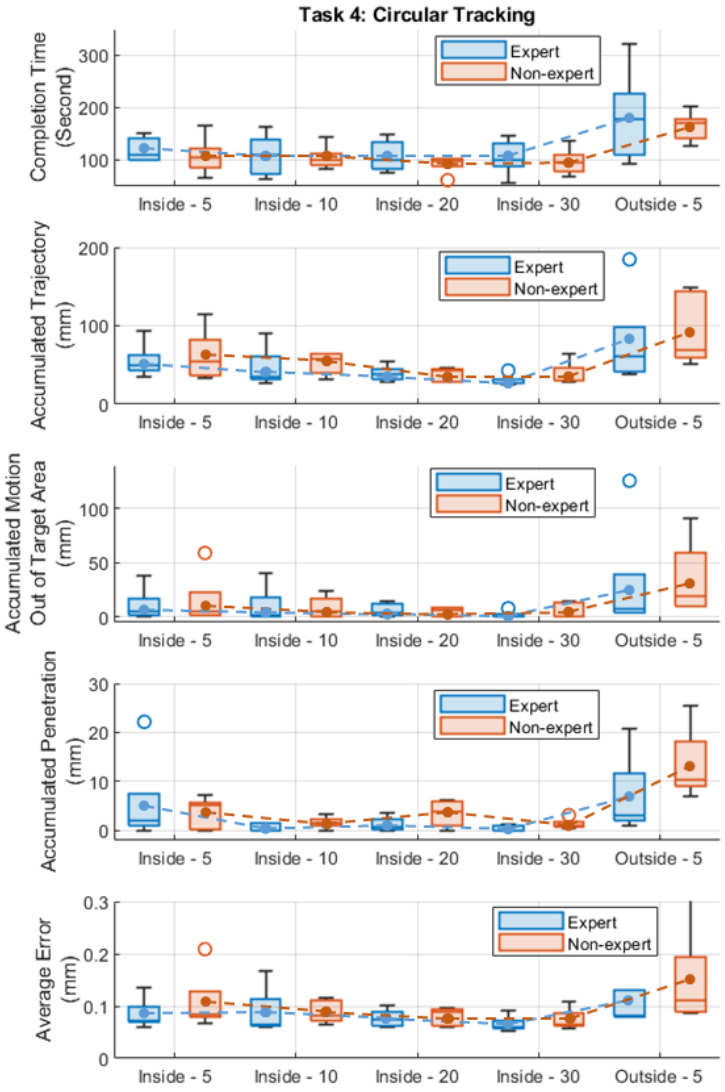

Figure 4.9. Performance for task 4.

To have an overall view we plot a radar chart of the score of each scaling factor in all four tasks (Fig. 4.10). The scoring rule as follows: only expert group is included; for each metric, the best performance gets 5 point, the second gets 4, etc.; performance is ranked by mean value, for the same mean value a smaller standard deviation is considered better, if both mean value and standard deviation are the same it will be a tie of same points; total score of each scaling factor in each task is scaled in 10. From the radar chart, the overall performance indicates the best performance of scaling factor 20 and 30 followed by 10 and 5. The outside control mode has the lowest score. For task 1, since the operation is relatively simple, the smaller and more agile scaling factor of 10 has the highest score followed closely by scaling factor 20 and 30. For task 2, as a result of the increasing laboring effort of holding forceps open/close throughout the task, scaling factor 20, which is neither very sensitive to master arm motion nor requiring large traveling of master arm, has an obvious superior performance. For task 3 which is focused mainly on stability of the control, inside 20 and 30 have equally good performance that leads with a large margin. For task 4, inside 30 has a clear advantage in avoiding error operating in the limited ring-shape task region.

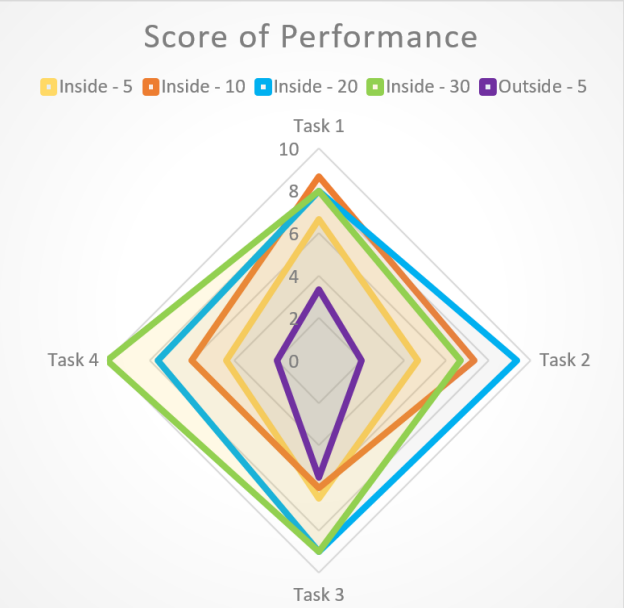

Figure 4.10. Score of performance.

4.4. Conclusions

Teleoperation control in vitreoretinal surgery is a developing technology. There are different control methods as inside control of the tool tip or outside control like in a conventional surgery. Besides, the scaling of control in the vitreoretinal surgery environment may have a major impact on the performance. Therefore, in this research we design 4 tasks that cover all fundamental operations in eye surgery to test the performance of the two different control modes in various scaling factors. The test result indicates an advantage of inside control mode with a large scaling factor compared to the outside control with limited scaling capability. In the meanwhile, the result reveals the possibility of different optimal scaling factors with respect to each individual task due to the nature of motions. The next step of the research is to investigate the performance with different types of feedback such as sound feedback and haptic feedback.

Chapter 5

Conclusions and future work

Conclusions for this dissertation

Robotics technology has been proved accurate and reliable in the industry of manufacturing, and therefore is regarded as potential solutions to many clinical issues in the field of dental and eye surgery. The result of this study is of significance as it verifies the capability of higher level automation in dental implant surgery, tooth preparation in crowning, as well as optimized performance in teleoperation control. The major conclusions from this dissertation are as follows:

- A proper AI decision system can be built by following the logic of a surgeon's behavior as a guidance in terms of automating the full process of the surgery under circumstances of unexpected contact or interaction between robot and patient during the surgery. The robot can finish the task while reacting to some of the common behaviors from the patient such as slight motions or requesting stop, as well as unknown behavior in case of emergency.
- As demanded by the fact of interaction between human and robot, an SMASC algorithm is developed in order to switch between various types of behaviors in real time such as position tracking, trajectory tracking, force tracking, and passive motion. The algorithm takes advantage of the linearity of PID admittance control in intuitive design for control gains and the non-linearity of SMC in a fast and smooth convergence.
- CAD/CAM technology can be utilized to compensate for the free hand error in conventional process of preparation. The design of trajectory based on the principal axis captures the precise contour of the tooth and therefore enables the robot to deliver a high quality cut to prepare for crowning.
- Robot has sufficient capability in preparing the tooth with a trade-off between speed and quality.

- Inside control has a clear advantage against the outside control with the VR environment of surgical training tasks.
- Scaling factor should be chosen according to the task and shall lie in a proper region, either too small or too large can yield decades in the surgeon's performance.

All the research efforts demonstrate that the robot system is capable of being implemented to the automation of surgery, and the teleoperation of typical tasks can be further improved according to the surgical task.

Future Work

Current studies have been focused on verifying the fundamental theories with a controlled lab experiment environment rather than a clinical environment. Therefore, based on these studies, the following future efforts are recommended:

- Data-based analysis on patient behavior in dental implant surgery for more precision decision making process design.
- Quantitative experiment on the implant drilling test with simulation on the biological motion of the patient with the full system.
- Quantitative analysis on the milling result of the tooth preparation comparing to the conventional result
- A complete design for the tooth preparation system including a full milling path design, and investigation of registration error.
- Further test on performance of VR simulation environment of teleoperation control with haptic feedback.

References

1. M. S. Block, R. W. Emery, K. Lank, and J. Ryan, "Implant Placement Accuracy Using Dynamic Navigation.", Int J Oral Maxillofac Implants, vol. 32, pp. 92–99, 2017.

2. T. Fortin, G. Champleboux, S. Bianchi, H. Buatois, and J. L. Coudert, "Precision of transfer of preoperative planning for oral implants based on cone-beam CT-scan images through a robotic drilling machine.", Clin Oral Implants Res, vol. 13, pp. 651–6, 2002.Nuytten, Thomas, Bert Claessens, Kristof Paredis, Johan Van Bael, and Daan Six. "Flexibility of a combined heat and power system with thermal energy storage for district heating." *Applied Energy* 104 (2013): 583-591

3. X. Sun, F. D. McKenzie, S. Bawab, J. Li, Y. Yoon, and J. K. Huang, "Automated dental implantation using image-guided robotics: registration results.", Int J Comput Assist Radiol Surg, vol. 6, pp. 627–34, 2011.

4. Kang-jie Cheng, Tian-shu Kan, Yun-feng Liu, Wei-dong Zhu, Fu-dong Zhu,Wei-binWang, Xian-feng Jiang, Xing-tao Dong, "Accuracy of dental implant surgery with robotic position feedback and registration algorithm: An in-vitro study.", Computers in Biology and Medicine, vol. 129, p. 104153, Feb. 2021, doi: 10.1016/j.compbiomed.2020.104153.

5. X. Sun, Y. Yoon, J. Li, and F. D. McKenzie, "Automated image-guided surgery for common and complex dental implants", Journal of Medical Engineering & Technology, vol. 38, no. 5, pp. 251–259, May 2014, doi: 10.3109/03091902.2014.913079.

6. Y. Wu, F. Wang, S. Fan, and J. K.-F. Chow, "Robotics in Dental Implantology", Oral and Maxillofacial Surgery Clinics of North America, vol. 31, no. 3, pp. 513–518, Aug. 2019, doi: 10.1016/j.coms.2019.03.013.

7. P. A. Lasota, T. Fong, and J. A. Shah, "A Survey of Methods for Safe Human-Robot Interaction", Foundations and Trends in Robotics, vol. 5, no. 3, pp. 261–349, 2017, doi: 10.1561/2300000052.R. E. Wirz, "Low-cost thermal energy storage for dispatchable CSP: Critical Project Review Report (No. EPC-14-003)," University of California at Los Angeles, Los Angeles, CA. (Publicly Available by Request to California Energy Commission), 2017.

8. D. P. Losey, C. G. McDonald, E. Battaglia, and M. K. O'Malley, "A Review of Intent Detection Arbitration, and Communication Aspects of Shared Control for Physical Human–Robot Interaction", Applied Mechanics Reviews, vol. 70, no. 1, Jan. 2018, doi: 10.1115/1.4039145.Gil,

Antoni, Marc Medrano, Ingrid Martorell, Ana Lázaro, Pablo Dolado, Belén Zalba, and Luisa F. Cabeza. "State of the art on high temperature thermal energy storage for power generation. Part 1—Concepts, materials and modellization." *Renewable and Sustainable Energy Reviews* 14, no. 1 (2010): 31-55.

9. A. Q. L. Keemink, H. van der Kooij, and A. H. A. Stienen, "Admittance control for physical human–robot interaction", The International Journal of Robotics Research, vol. 37, no. 11, pp. 1421–1444, Apr. 2018, doi: 10.1177/0278364918768950.Hasnain, S. M. "Review on sustainable thermal energy storage technologies, Part I: heat storage materials and techniques." *Energy conversion and management* 39.11 (1998): 1127-1138.

10. F. Ferraguti, C. T. Landi, L. Sabattini, M. Bonf`e, C. Fantuzzi, and C. Secchi, "A variable admittance control strategy for stable physical human–robot interaction", The International Journal of Robotics Research, vol. 38, no. 6, pp. 747–765, Apr. 2019, doi: 10.1177/0278364919840415.

11. I.S.O. 10218-1:2011, Robots and robotic devices — Safety requirements for industrial robots — Part 1: Robots. International Organization for Standardization, 2011.

12. I.S.O. 10218-2:2011, Robots and robotic devices — Safety requirements for industrial robots — Part 2: Robot systems and integration. International Organization for Standardization, 2011.

13. I.S.O. 14971:2019, Medical devices — Application of risk management to medical devices. International Organization for Standardization, 2019.

14. Sugiura, Hisashi, et al. "REACTIVE SELF COLLISION AVOIDANCE WITH DYNAMIC TASK PRIORITIZATION FOR HUMANOID ROBOTS." International Journal of Humanoid Robotics, vol. 07, no. 01, Mar. 2010, pp. 31–54. DOI.org (Crossref), doi:10.1142/S0219843610001976.

15. Yu, Biao, and Prabhakar R. Pagilla. "Design and Implementation of a Robust Switching Control Scheme for a Class of Constrained Robot Tasks." International Journal of Systems Science, vol. 37, no. 5, Apr. 2006, pp. 303–21. DOI.org (Crossref), doi:10.1080/00207720600566941.

16. Delgado, Raimarius, et al. "Real-Time Control Architecture Based on Xenomai Using ROS Packages for a Service Robot." Journal of Systems and Software, vol. 151, May 2019, pp. 8–19. DOI.org (Crossref), doi:10.1016/j.jss.2019.01.052.

17. V. Utkin, J. Guldner, and J. Shi, Sliding Mode Control in Electro-Mechanical Systems. CRC Press, 2017.

18. H. Li, P. Shi, D. Yao, and L. Wu, "Observer-based adaptive sliding mode control for nonlinear Markovian jump systems", Automatica, vol. 64, pp. 133–142, Feb. 2016, doi: 10.1016/j.automatica.2015.11.007.

19. P. Polygerinos, Z. Wang, K. C. Galloway, R. J. Wood, and C. J. Walsh, "Soft robotic glove for combined assistance and at-home rehabilitation", Robotics and Autonomous Systems, vol. 73, pp. 135–143, Nov. 2015, doi: 10.1016/j.robot.2014.08.014.

20. J. E. Solanes, L. Gracia, P. Mu˜noz-Benavent, J. V. Miro, M. G. Carmichael, and J. Tornero, "Human–robot collaboration for safe object transportation using force feedback", Robotics and Autonomous Systems, vol. 107, pp. 196–208, Sep. 2018, doi: 10.1016/j.robot.2018.06.003.

21. V. Utkin and J. Shi, "Integral sliding mode in systems operating under uncertainty conditions", in Proceedings of 35th IEEE Conference on Decision and Control, doi: 10.1109/cdc.1996.577594.

22. F. Castanos and L. Fridman, "Analysis and Design of Integral Sliding Manifolds for Systems With Unmatched Perturbations", IEEE Transactions on Automatic Control, vol. 51, no. 5, pp. 853–858, May 2006, doi: 10.1109/tac.2006.875008.

23. A. Wege, K. Kondak, and G. Hommel, "Force Control Strategy for a Hand Exoskeleton Based on Sliding Mode Position Control", in 2006 IEEE/RSJ International Conference on Intelligent Robots and Systems, 2006, doi: 10.1109/iros.2006.282169.

24. R. Kikuuwe, "Some stability proofs on proxy-based sliding mode control", IMA Journal of Mathematical Control and Information, vol. 35, no. 4, pp. 1319–1341, Jul. 2017, doi: 10.1093/imamci/dnx030.

25. J. E. Solanes, L. Gracia, P. Mu˜noz-Benavent, A. Esparza, J. V. Miro, and J. Tornero, "Adaptive robust control and admittance control for contact-driven robotic surface conditioning", Robotics and Computer-Integrated Manufacturing, vol. 54, pp. 115–132, Dec. 2018, doi: 10.1016/j.rcim.2018.05.003.

26. Li, Zhi-Jing, et al. "A Position and Torque Switching Control Method for Robot Collision Safety." International Journal of Automation and Computing, vol. 15, no. 2, Apr. 2018, pp. 156–68. DOI.org (Crossref), doi:10.1007/s11633-017-1104-9.

27. Charles J. Goodacre, Wayne V. Campagni, Steven A. Aquilino. Tooth preparations for complete crowns: An art form based on scientific principles. The Journal of Prosthetic Dentistry 85, 363–376 Elsevier BV, 2001.

28. Amanda Maria de Oliveira Dal Piva, João Paulo Mendes Tribst, Ernesto Byron Benalcázar Jalkh, Lilian Costa Anami, Estevam Augusto Bonfante, Marco Antonio Bottino. Minimal tooth preparation for posterior monolithic ceramic crowns: Effect on the mechanical behavior reliability and translucency. Dental Materials 37, e140–e150 Elsevier BV, 2021.

29. Dr. Shabana Lone. "Tooth Preparation, Impression Technique, Provisionalization and Bonding PFZ Crown for Restoring Endodontically Treated Tooth: A Case Report" MAR Dental Sciences 2.2 (2021)

30. Katsushi Katano, Kazunori Nakajima, Maho Saito, Yoshiaki Kawano, Tomotaka Takeda, Kenichi Fukuda. Effects of Line of Vision on Posture Muscle Activity and Sitting Balance During Tooth Preparation. International Dental Journal 71, 399–406 Elsevier BV, 2021.

31. Sebastian Baumgaertel, J. Martin Palomo, Leena Palomo, Mark G. Hans. Reliability and accuracy of cone-beam computed tomography dental measurements. American Journal of Orthodontics and Dentofacial Orthopedics 136, 19–25 Elsevier BV, 2009.

32. Bruno Pereira da Silva, Kyle Stanley, Jameel Gardee. Laminate veneers: Preplanning and treatment using digital guided tooth preparation. Journal of Esthetic and Restorative Dentistry 32, 150–160 Wiley, 2020.

33. Takafumi Otani, Ariel J. Raigrodski, Lloyd Mancl, Ikuru Kanuma, Jacob Rosen. In vitro evaluation of accuracy and precision of automated robotic tooth preparation system for porcelain laminate veneers. The Journal of Prosthetic Dentistry 114, 229–235 Elsevier BV, 2015.

34. Ning Dai, Yicheng Zhong, Hao Liu, Fusong Yuan, Yuchun Sun. Digital modeling technology for full dental crown tooth preparation. Computers in Biology and Medicine 71, 190–197 Elsevier BV, 2016.

35. Tom C.T. van Riet, Kevin T.H. Chin Jen Sem, Jean-Pierre T.F. Ho, René Spijker, Jens Kober, Jan de Lange. Robot technology in dentistry part two of a systematic review: an overview of initiatives. Dental Materials 37, 1227–1236 Elsevier BV, 2021.

36. Fusong Yuan, Peijun Lyu. A preliminary study on a tooth preparation robot. Advances in Applied Ceramics 119, 332–337 Informa UK Limited, 2019.

37. Jingang Jiang, Yafeng Guo, Zhiyuan Huang, Yongde Zhang, Dianhao Wu, Yi Liu. Adjacent surface trajectory planning of robot-assisted tooth preparation based on augmented reality. Engineering Science and Technology an International Journal 27, 101001 Elsevier BV, 2022.

38. Goldenberg, D., Shahar, J., Loewenstein, A., & Goldstein, M. (2013). Diameters of retinal blood vessels in a healthy cohort as measured by spectral domain optical coherence tomography. Retina, 33(9), 1888-1894.

39. Gonenc, B., Tran, N., Riviere, C. N., Gehlbach, P., Taylor, R. H., & Iordachita, I. (2015, September). Force-based puncture detection and active position holding for assisted retinal vein cannulation. In 2015 IEEE International Conference on Multisensor Fusion and Integration for Intelligent Systems (MFI)(pp. 322-327). IEEE.

40. Channa, R., Iordachita, I., & Handa, J. T. (2017). Robotic eye surgery. Retina (Philadelphia, Pa.), 37(7), 1220.

41. Gupta, P. K., Jensen, P. S., & de Juan, E. (1999, September). Surgical forces and tactile perception during retinal microsurgery. In International conference on medical image computing and computer-assisted intervention (pp. 1218-1225). Springer, Berlin, Heidelberg.

42. Patkin, M. (1967). Ergonomic aspects of surgical dexterity. The Medical Journal of Australia, 2(17), 775-777.

43. Singh, S. P. N., & Riviere, C. N. (2002, April). Physiological tremor amplitude during retinal microsurgery. In Proceedings of the IEEE 28th Annual Northeast Bioengineering Conference (IEEE Cat. No. 02CH37342) (pp. 171-172). IEEE.

44. Jacobsen, M. F., Konge, L., Alberti, M., La Cour, M., Park, Y. S., & Thomsen, A. S. S. (2020). Robot-assisted vitreoretinal surgery improves surgical accuracy compared with manual surgery: a randomized trial in a simulated setting. Retina (Philadelphia, Pa.), 40(11), 2091.)

45. de Smet, M. D., de Jonge, N., Iannetta, D., Faridpooya, K., van Oosterhout, E., Naus, G., ... & Beelen, M. J. (2019). Human/robotic interaction: vision limits performance in simulated vitreoretinal surgery. Acta ophthalmologica, 97(7), 672-678).

46. Maberley, D. A., Beelen, M., Smit, J., Meenink, T., Naus, G., Wagner, C., & de Smet, M. D. (2020). A comparison of robotic and manual surgery for internal limiting membrane peeling. Graefe's Archive for Clinical and Experimental Ophthalmology, 258(4), 773-778.

47. Tsirbas, A., Mango, C., & Dutson, E. (2007). Robotic ocular surgery. British journal of ophthalmology, 91(1), 18-21.

48. Bourges, J. L., Hubschman, J. P., Burt, B., Culjat, M., & Schwartz, S. D. (2009). Robotic microsurgery: corneal transplantation. British journal of ophthalmology, 93(12), 1672-1675.

49. Hubschman, J., Bourla, D., Tsirbas, A., Culjat, M., Dutson, E., Kreiger, A. E., & Schwartz, S. D. (2007). Robotic vitreoretinal surgery. Investigative Ophthalmology & Visual Science, 48(13), 6030-6030.

50. Constable IJ. Robotic ocular ultramicrosurgery. Aust N Z J Ophthalmol 1998.

51. Bourla, D. H., Hubschman, J. P., Culjat, M., Tsirbas, A., Gupta, A., & Schwartz, S. D. (2008). Feasibility study of intraocular robotic surgery with the da Vinci surgical system. Retina, 28(1), 154-158.

52. Rahimy, E., Wilson, J., Tsao, T. C., Schwartz, S., & Hubschman, J. P. (2013). Robot-assisted intraocular surgery: development of the IRISS and feasibility studies in an animal model. Eye, 27(8), 972-978.

53. R. Parasuraman, T. B. Sheridan, and C. D. Wickens, "A model for types and levels of human interaction with automation", IEEE Transactions on Systems Man, and Cybernetics - Part A: Systems and Humans, vol. 30, no. 3, pp. 286–297, May 2000, doi: 10.1109/3468.844354.

54.] J. E. Lee, B. A. Gozen, and O. B. Ozdoganlar, "Modeling and experimentation of bone drilling forces", Journal of Biomechanics, vol. 45, no. 6, pp. 1076–1083, Apr. 2012, doi: 10.1016/j.jbiomech.2011.12.012.

55. W.-Y. Lee, C.-L. Shih, and S.-T. Lee, "Force Control and Breakthrough Detection of a Bone-Drilling System", IEEE/ASME Transactions on Mechatronics, vol. 9, no. 1, pp. 20–29, Mar. 2004, doi: 10.1109/tmech.2004.823850.